LA-UR-22-24878

Approved for public release; distribution is unlimited.

Title:	Electron Drift Kinetics in Space and in the Lab
Author(s):	Wetherton, Blake Alastair
Intended for:	Job Talk at LLNL
Issued:	2022-05-25

Electron Drift Kinetics in Space and in the Lab

Blake Wetherton
Collaborators:
J. Egedal, A. Le, W. Daughton, P. Montag,
C. Forest, A. Stanier, S. Boldyrev

5/31/2022

LA-UR-

Overview

- Drift Kinetics Overview
- Magnetic Reconnection
  - Introduction/Background
  - Description of Anisotropic Model
  - Validating the Model with Spacecraft Data
  - Importance of Mass Ratio in Kinetic Simulations
  - Prediction of Scaling of Electron Heating
- Drift Kinetic Method for Gradient Estimation in Space Plasma
  - Agyrotropy in Magnetized Plasmas
  - Relating Gradients to Agyrotropy
  - Model Derivation/Results
  - Verification on Simulation Data
- Magnetic Mirrors
  - Introduction/Background on Mirrors
  - Overview of the Drift-Kinetic Model
  - Application to Deuterium Device
  - Development of the Sheath Potential
  - Particle-in-Cell Simulations
  - Adding in Sloshing Ion Beams

Overview

- **Drift Kinetics Overview**
- Magnetic Reconnection
  - Introduction/Background
  - Description of Anisotropic Model
  - Validating the Model with Spacecraft Data
  - Importance of Mass Ratio in Kinetic Simulations
  - Prediction of Scaling of Electron Heating
- Drift Kinetic Method for Gradient Estimation in Space Plasma
  - Agyrotropy in Magnetized Plasmas
  - Relating Gradients to Agyrotropy
  - Model Derivation/Results
  - Verification on Simulation Data
- Magnetic Mirrors
  - Introduction/Background on Mirrors
  - Overview of the Drift-Kinetic Model
  - Application to Deuterium Device
  - Development of the Sheath Potential
  - Particle-in-Cell Simulations
  - Adding in Sloshing Ion Beams

Drift Kinetics Overview

- In a magnetized plasma, dynamics are fundamentally split between the directions parallel and perpendicular to the magnetic field
- Generally, gyration about the magnetic field will occur on smaller spatial and time scales than the bulk dynamics of the system
- From Hamiltonian mechanics, a periodic motion on a time scale much shorter than the other system dynamics leads to an adiabatic invariant
- The adiabatic invariant for this motion is the magnetic moment $\mu = \frac{m{v_\perp}^2}{2B}$, which will be approximately conserved

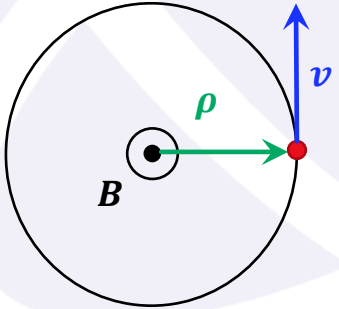

Drift Kinetics Overview

- Drift kinetics integrates out the fast gyromotion and employs the conserved μ, i.e. $f(\boldsymbol{x}, v_{||}, v_{\perp}, \gamma, t) \rightarrow \bar{f}\ (\boldsymbol{x}, U, \mu, t)$
- Models a distribution of guiding centers, where $\boldsymbol{v}_{gc} = v_{||}\hat{b} + \boldsymbol{v}_D$

$$\mathbf{v}_D = \frac{\mathbf{E} \times \mathbf{B}}{B^2} - \frac{1}{\Omega_e}\mathbf{b} \times \left(\frac{\mu}{m}\boldsymbol{\nabla} B + v_{\|}^2 (\mathbf{b} \cdot \boldsymbol{\nabla})\mathbf{b} + v_{\|}\frac{\partial \mathbf{b}}{\partial t} \right)$$

- For reconnection and mirrors, we can often model a flux tube in a collisionless fast-streaming limit where $v_{the} \gg v_D$
- This allows for a Liouville mapping from a local distribution in the flux tube to an upstream source distribution that conserves μ along particle trajectories.

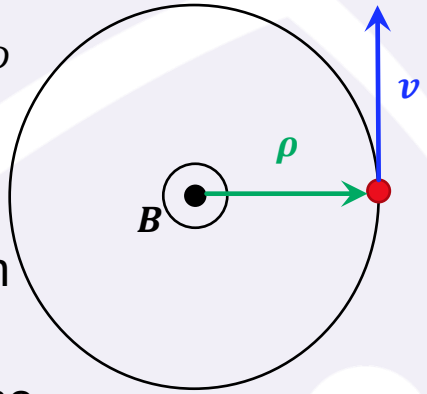

Overview

- Drift Kinetics Overview
- **Magnetic Reconnection** [Wetherton+,GRL, 2019]
  - Introduction/Background
  - Description of Anisotropic Model
  - Validating the Model with Spacecraft Data
  - Importance of Mass Ratio in Kinetic Simulations
  - Prediction of Scaling of Electron Heating
- Drift Kinetic Method for Gradient Estimation in Space Plasma
  - Agyrotropy in Magnetized Plasmas
  - Relating Gradients to Agyrotropy
  - Model Derivation/Results
  - Verification on Simulation Data
- Magnetic Mirrors
  - Introduction/Background on Mirrors
  - Overview of the Drift-Kinetic Model
  - Application to Deuterium Device
  - Development of the Sheath Potential
  - Particle-in-Cell Simulations
  - Adding in Sloshing Ion Beams

Magnetic Reconnection

- A change in magnetic topology
- Field lines break and reconnect
- Magnetic energy is released and transferred to
  - Thermal energy
  - Kinetic energy of nonthermal particles
  - Kinetic energy in large scale flows

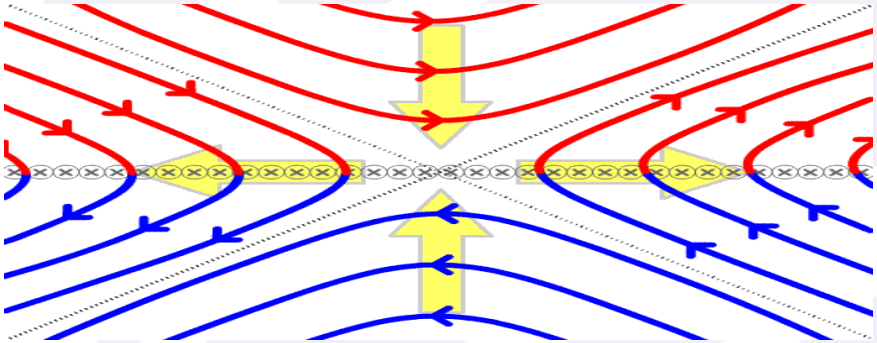

Animation: Wikipedia

Space Weather

- The solar wind affects Earth's environment
- Magnetic reconnection mediates the coupling

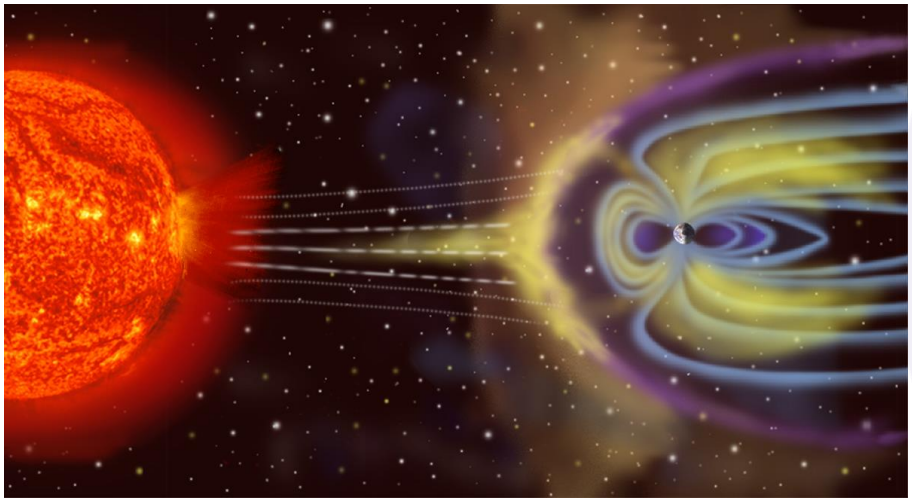

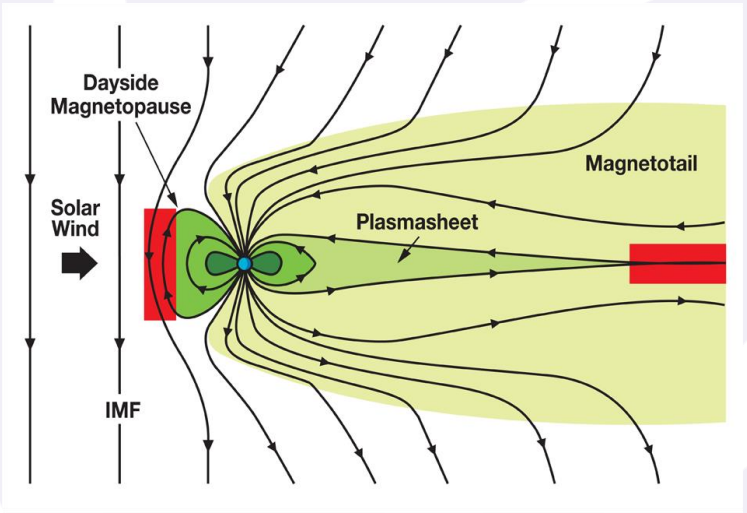

Image Credit: NASA

Scales of Reconnection

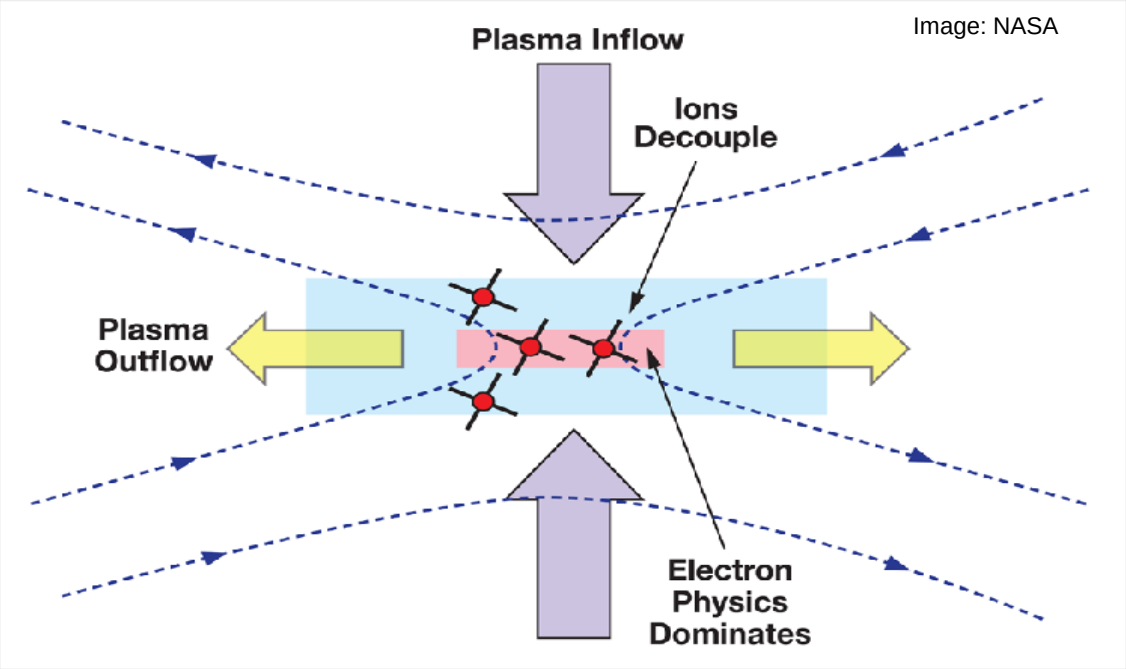

Plasma Kinetic Description

The collisionless Vlasov equation:

$$\left(\frac{\partial}{\partial t} + \mathbf{v} \right. \left. \frac{d}{dt} f_j(\mathbf{x}, \mathbf{v}, t) = 0 \right) \cdot \nabla_v \Big) f_j = 0$$

$$n_j = \int f_j d^3v \qquad \mathbf{J}_j = q_j \int \mathbf{v} f_j d^3v$$

\+ Maxwell's eqs.

Vlasov-Maxwell system of equations

Can be solved numerically (PIC-codes)

Fluid Formulation (Conservation Laws)

mass:

$$\frac{\partial n}{\partial t} + \frac{\partial (n u_j)}{\partial x_j} = 0,$$

momentum:

Sweet-Parker

$$mn\left(\frac{\partial u_j}{\partial t} + u_k \frac{\partial u_j}{\partial x_k}\right) + \frac{\partial P_{jk}}{\partial x_k} - en(E_j + \epsilon_{jkl} u_k B_l) - F_j^{\text{coll}} = 0,$$

energy:

$$\frac{\partial P_{jk}}{\partial t} + \frac{\partial}{\partial x_l}(P_{jk} u_l + Q_{jkl}) + \frac{\partial u_{[j}}{\partial x_l} P_{lk]} = \frac{e}{m} \epsilon_{[jlm} B_m P_{lk]} - G_{jk}^{\text{coll}} = 0$$

.
.
.

Isotropic (scalar) pressure is a standard closure

$$p = n T$$

Add Maxwell's eqs to complete the fluid model

Two-Fluid Simulation vs. Kinetic

Out of plane current

Isotropic pressure

Kinetic Simulation

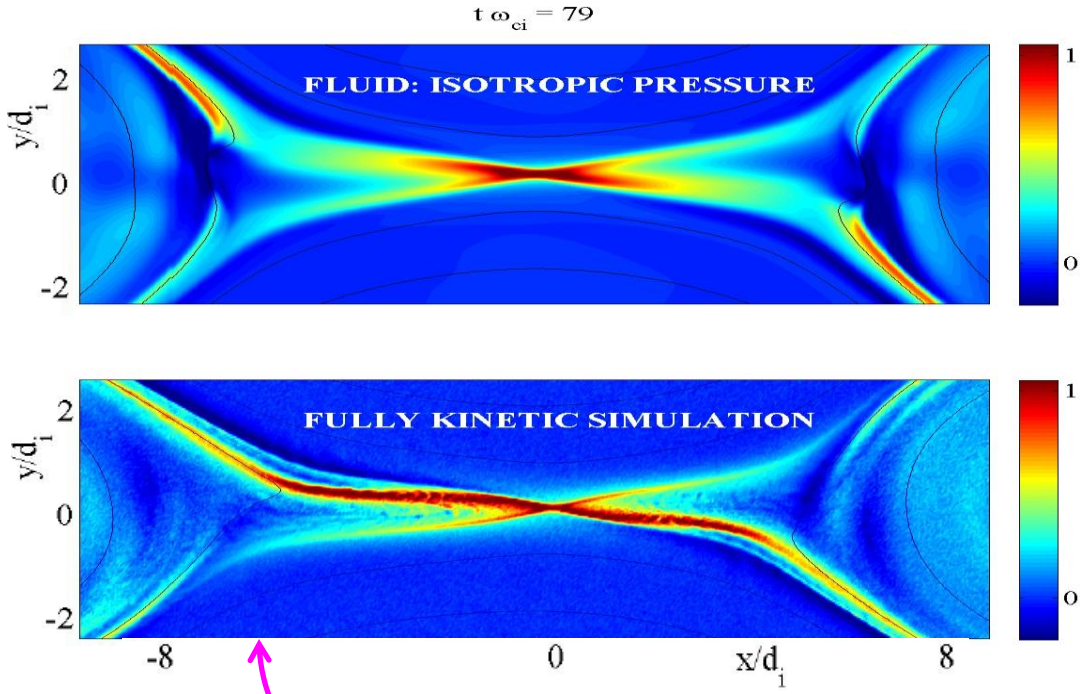

Particle In Cell (PIC) simulation,

Pressure Anisotropy

- WIND Spacecraft Observations in Magnetotail, 60R_E
  - Measurements within the ion diffusion region reveal:
    Strong anisotropy in f_e
    $p_{||} > p_{\perp}$

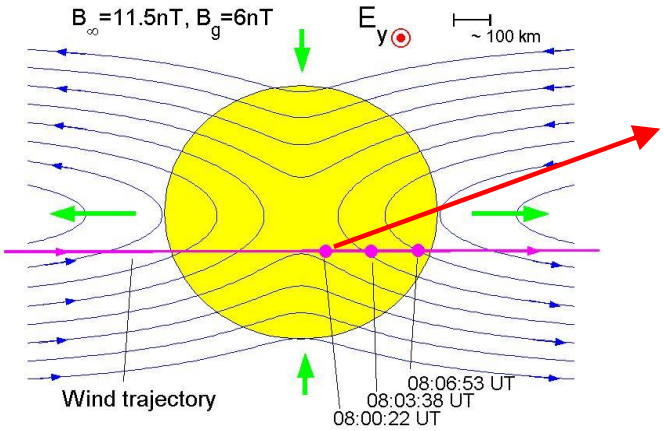

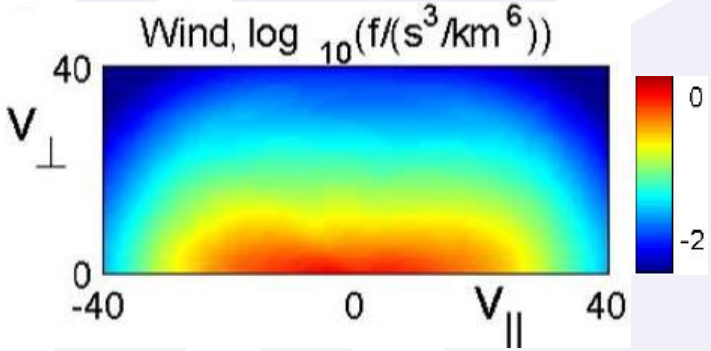

Kinetic Model of Electron Dynamics

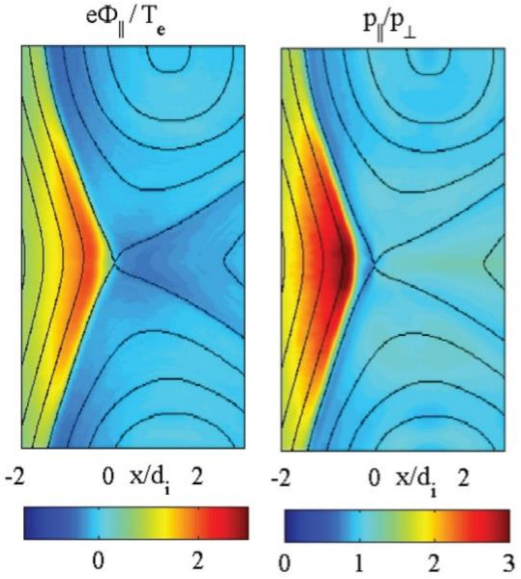

[Fig 10, Egedal+, POP, 2011]

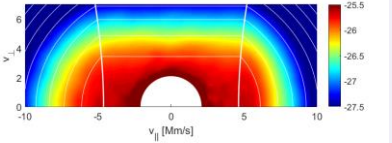

MMS data, 10/31/15
(magnetopause)

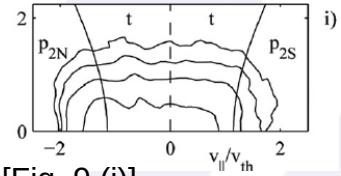

[Fig. 9 (i)]

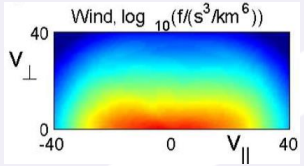

[Øieroset+, PRL, 2001]
(magnetotail)

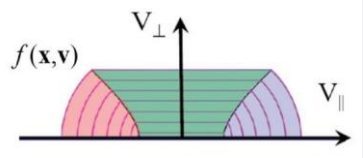

[Egedal+, PRL,2005, JGR,2008]

$$f(\mathbf{x},\mathbf{v}) = \begin{cases} f_\infty(\mathcal{E} - e\Phi_\parallel) & , \text{ passing} \\ f_\infty(\mu B_\infty) & , \text{ trapped} \end{cases}$$

Egedal+, JGR (2009), PoP (2013)

Electrons in an Expanding Flux Tube

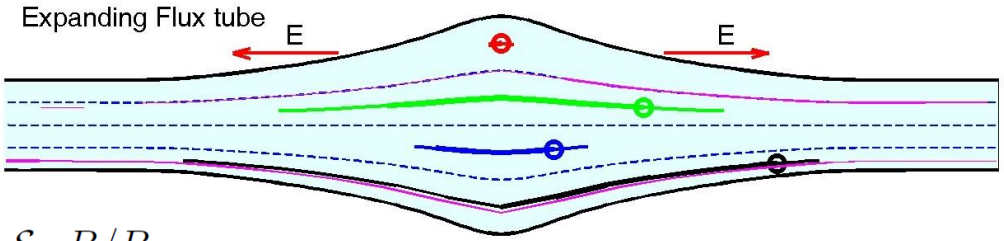

Trapped:

$$\mathcal{E}_\perp = \mu B = \mathcal{E}_\infty B/B_\infty$$

$$\Longrightarrow \quad \mathcal{E}_\infty = \mu B_\infty$$

Passing:

$$\mathcal{E} = \mathcal{E}_\infty + e\Phi_\parallel$$

$$\Longrightarrow \quad \mathcal{E}_\infty = \mathcal{E} - e\Phi_\parallel$$

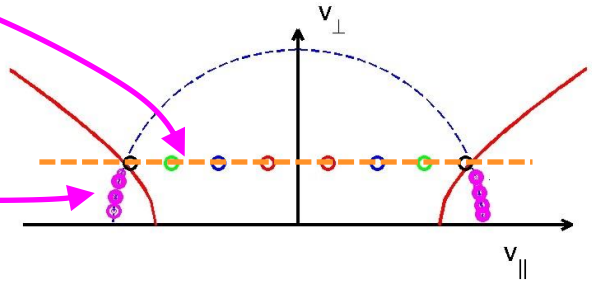

Vlasov:

$$\frac{df}{dt} = 0$$

$$f(\mathbf{x},\mathbf{v}) = f_\infty(\mathcal{E}_\infty)$$

$$f(\mathbf{x},\mathbf{v}) = \begin{cases} f_\infty(\mathcal{E} - e\Phi_\parallel) & , \text{ passing} \\ f_\infty(\mu B_\infty) & , \text{ trapped} \end{cases}$$

Egedal+, JGR (2009)

Fluid Closure and Equations of State

Boltzmann

CGL

$$\bar{\mathbf{P}} = p_i \bar{\mathbf{I}} + \bar{\mathbf{P}}_e = p_i \bar{\mathbf{I}} + p_\perp \bar{\mathbf{I}} + (p_\parallel - p_\perp)\frac{\mathbf{BB}}{B^2},$$

$$\tilde{p}_\parallel = \tilde{n}\frac{2}{2+\alpha} + \frac{\pi \tilde{n}^3}{6\tilde{B}^2}\frac{2\alpha}{2\alpha+1},$$

$$\tilde{p}_\perp = \tilde{n}\frac{1}{1+\alpha} + \tilde{n}\tilde{B}\frac{\alpha}{\alpha+1}.$$

Here, $\alpha = \tilde{n}^3/\tilde{B}^2$ and $\tilde{Q} = Q/Q_\infty$

Anisotropic pressure model

$$f(\mathbf{x},\mathbf{v}) = \begin{cases} f_\infty(\mathcal{E} - e\Phi_\parallel) & , \text{ passing} \\ f_\infty(\mu B_\infty) & , \text{ trapped} \end{cases}$$

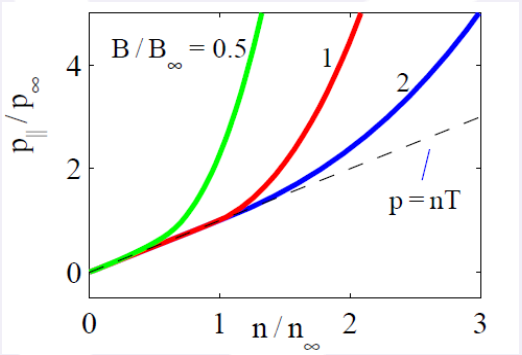

A. Le et al., PRL (2009)

$$\xrightarrow[\Phi_\parallel \gg T_e]{} \quad p_\parallel \propto \frac{n^3}{B^2}, \qquad p_\perp \propto nB$$

Smooth transition from Boltzmann to double adiabatic CGL-scaling

[G Chew, M Goldberger, F E Low, 1956]

Anisotropic EoS Implemented in Two-Fluid Code

Out of plane current

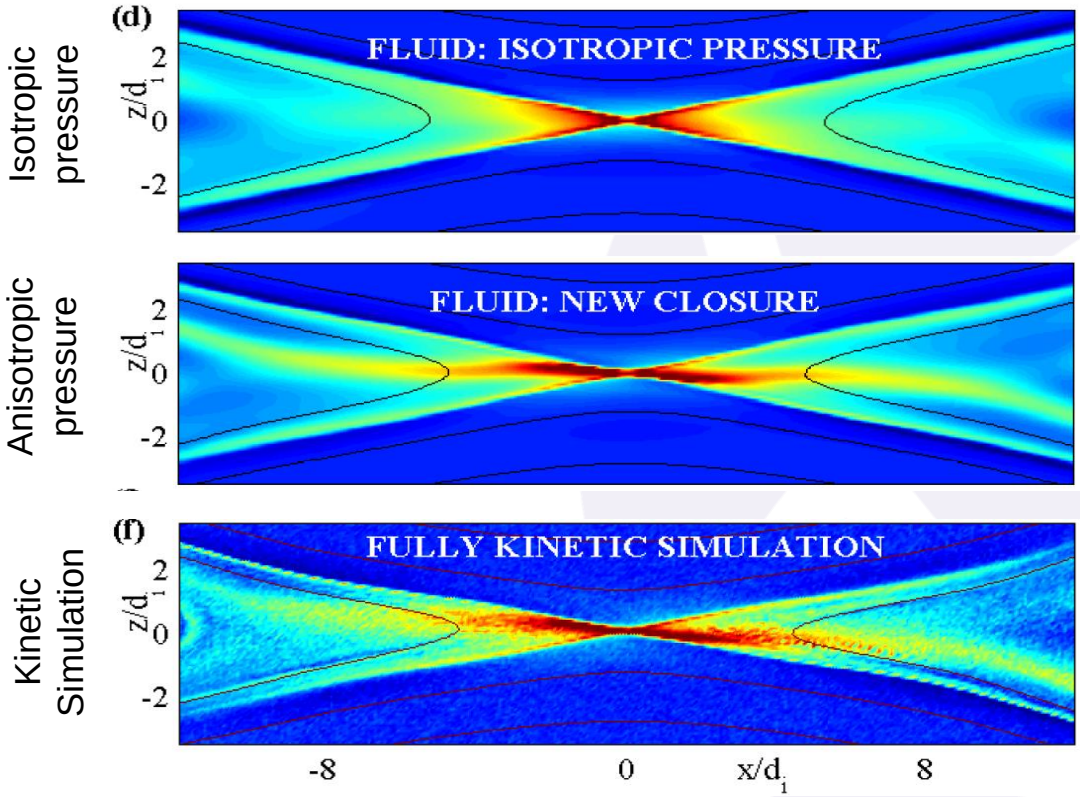

[Ohia+, 2012]

NASA's Magnetospheric Multiscale (MMS) Mission

Image Credits: NASA

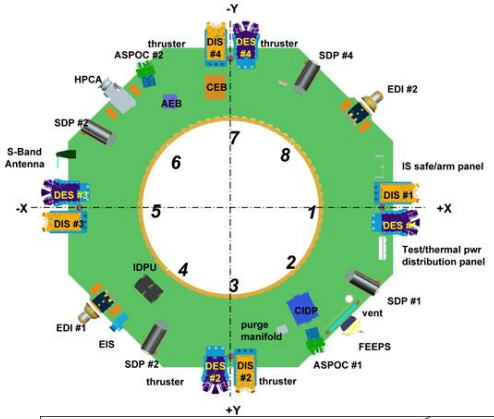

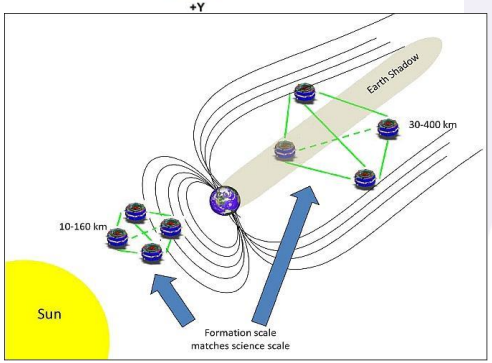

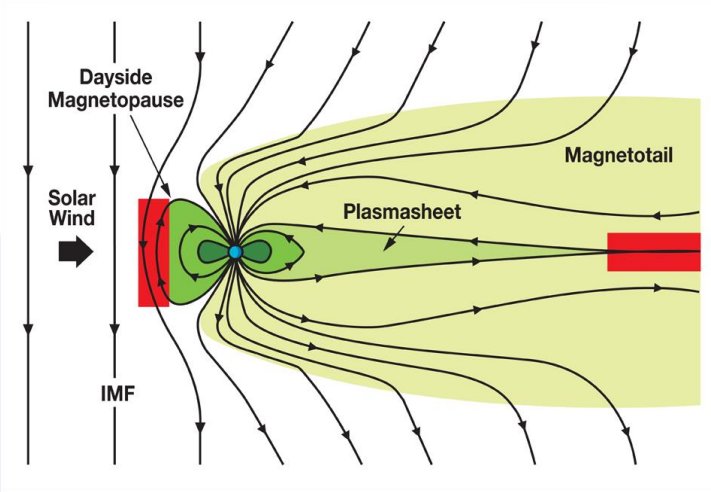

Model Tested Against MMS data

[Øieroset, GRL, 2016], $B_g \sim 2\ B_r$

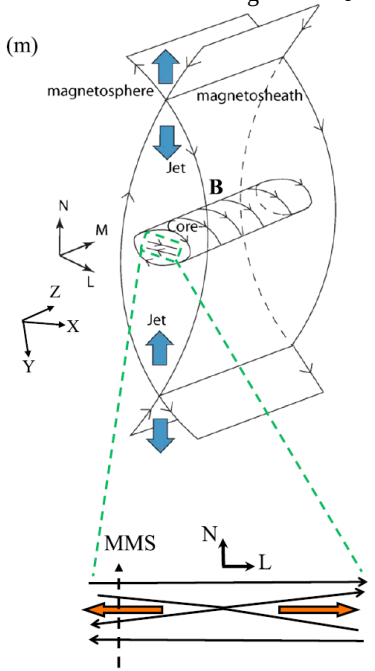

L ~ 10 d_i

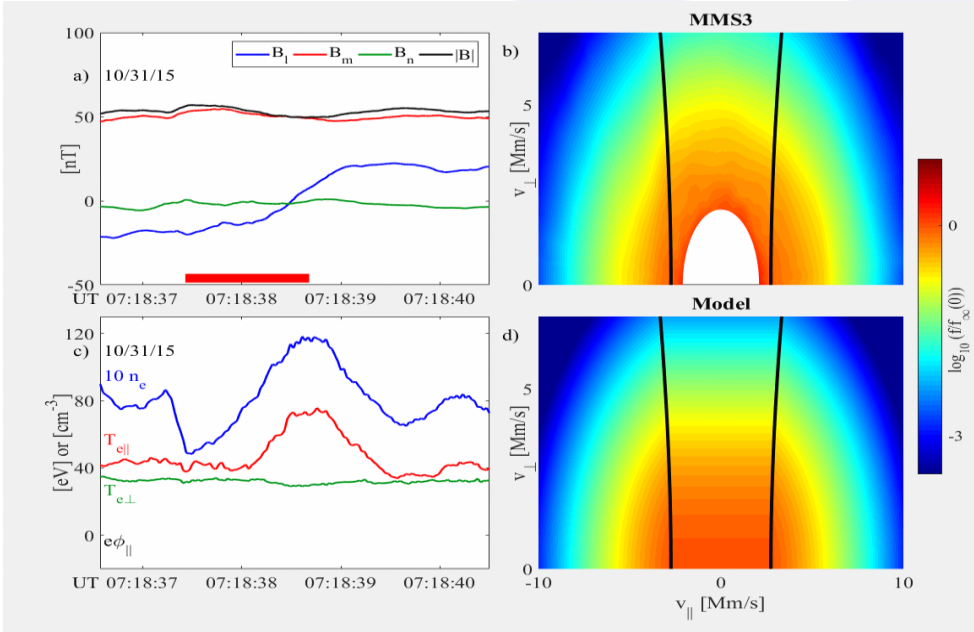

$$f(\mathbf{x},\mathbf{v}) = \begin{cases} f_\infty(\mathcal{E} - e\Phi_{||}) & , \text{ passing} \\ f_\infty(\mu B_\infty) & , \text{ trapped} \end{cases}$$

MMS Event: ~07:18 10/31/15

- MMS passed through the exhaust ~10 d_i from the x-line
- The event had a strong guide field, B_g ~ 2 B_r
- Distributions measured by MMS match the 1D flux tube model.

[Wetherton+, GRL, 2019]

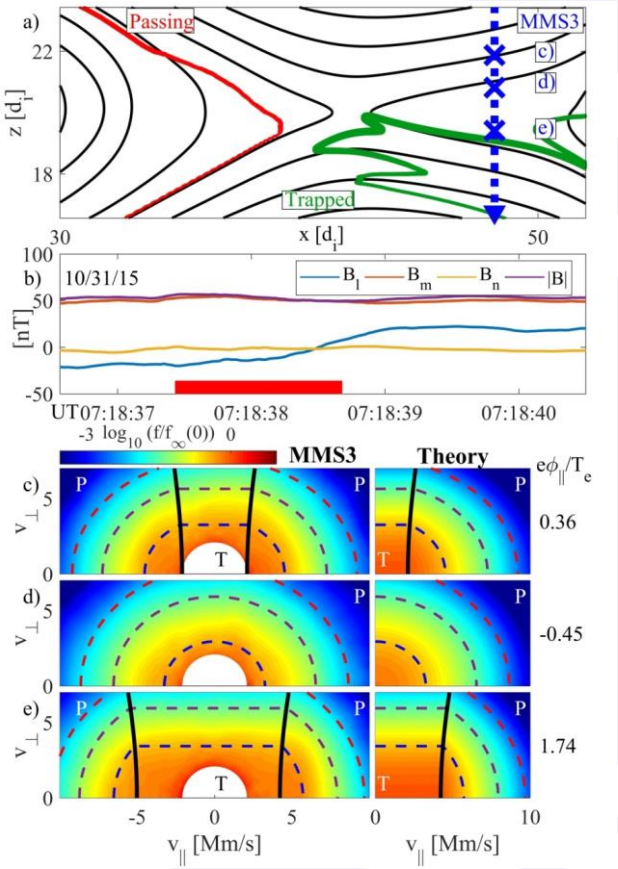

MMS Event: ~07:18 10/31/15

- Perpendicular electron temperature was roughly constant with strong parallel heating.
- The region from the density cavity to the density peak follows the Le 2009 EoS well.
- Scalings span from Boltzmann in the cavity to CGL at the peak.

[Wetherton+, GRL, 2019]

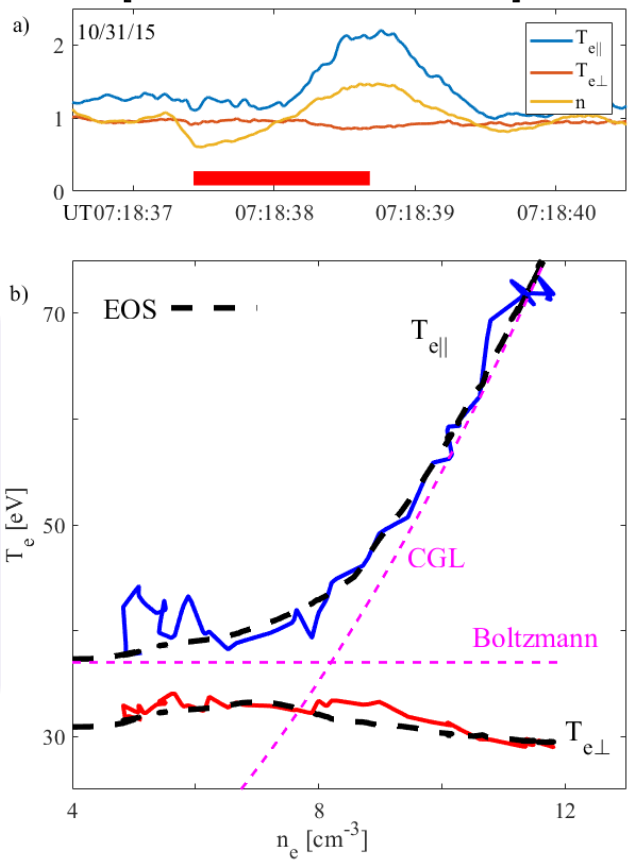

Comparison to H3D Hybrid Simulation

- H3D simulations can incorporate an anisotropic EoS to evolve the electron fluid
- The Le 2009 EoS in H3D reproduces the cut measured by MMS3 on 10/31/15, both qualitatively and quantitatively.

[Wetherton+, GRL, 2019]

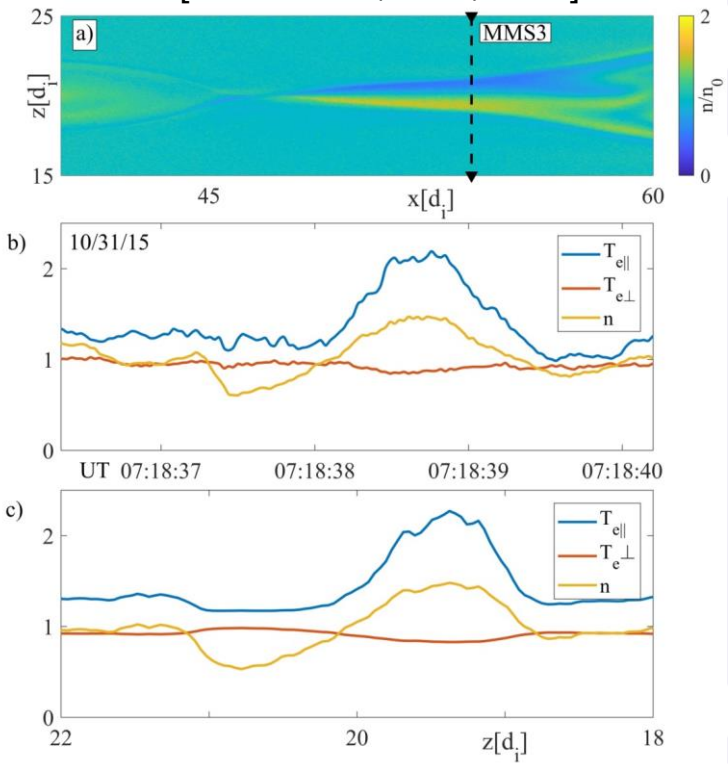

H3D vs. Low Mass Ratio PIC Simulations

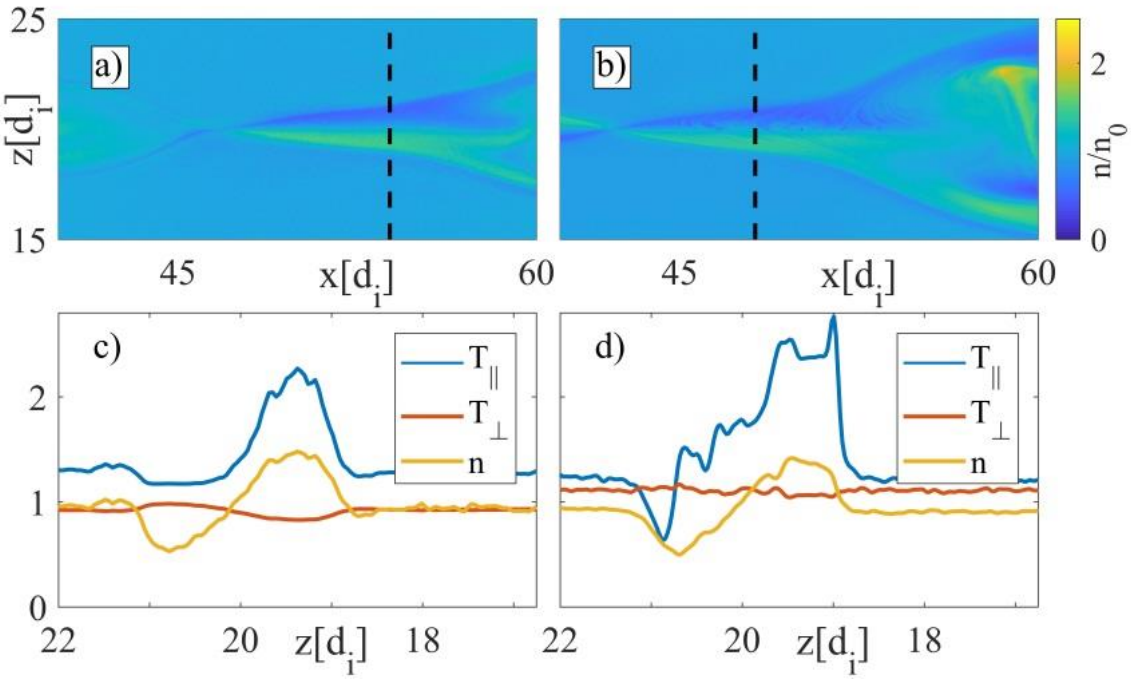

[Wetherton+, GRL, 2019]

Why does the kinetic simulation do worse?

- Using Hammett-Perkins closure, Boltzmann limit corresponds to $\omega/(k_{||}v_{\mathrm{th}}) \ll 1$ where $\omega/(k_{||}v_{\mathrm{th},e}) \simeq \sqrt{m_{\mathrm{e}}/m_{\mathrm{i}}}/\sqrt{\beta_e}$

- For typical magnetospheric parameters:
  $\omega/(k_{||}v_{\mathrm{th},e}) \simeq \sqrt{1/1,836}/\sqrt{0.1} \simeq 0.1 \ll 1$
- For reduced mass ratio 100, $\omega/(k_{||}v_{\mathrm{th},e}) \simeq 1$, and this is no longer in the Boltzmann limit
- The reduced electron thermal speed cannot provide adequate heat flux to keep the cavity in the Boltzmann limit

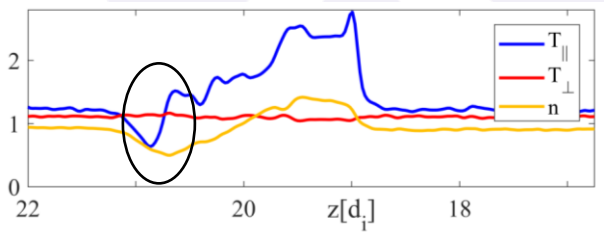

Exhaust Heating

- We can estimate the peak heating of the reconnection outflow with the Lê 2009 EoS and force balance across the reconnection layer, as was previously done in the low to moderate guidefield regimes (Le+, PoP, 2016; Ohia+,GRL, 2015)

$$\tilde{p}_{\parallel} = \tilde{n}\,\frac{2}{2+\alpha} + \frac{\pi\tilde{n}^3}{6\tilde{B}^2}\,\frac{2\alpha}{2\alpha+1},$$

$$\tilde{p}_{\perp} = \tilde{n}\,\frac{1}{1+\alpha} + \tilde{n}\tilde{B}\,\frac{\alpha}{\alpha+1}.$$

$$\tilde{n}^{\Gamma}\beta_{i\infty} + \tilde{p}_{e\perp}(\tilde{n},\tilde{B})\beta_{e\infty} + \tilde{B}^2 = 1 + \beta_{i\infty} + \beta_{e\infty}$$

Condition for Magnetic Field Strength

- One more equation is needed to solve for the outflow pressures given the inflow conditions
- In previous studies, this was the marginal firehose condition
- The marginal firehose condition is typically not approached in strong guide field reconnection
- We approximate the condition for peak heating the in-plane field vanishing, leaving only the guide field strength

$$\tilde{B} = \frac{B_g}{\sqrt{B_r^2 + B_g^2}}$$

Asymptotic Scaling

- Asymptotically, it follows that:

$$\text{For } \beta_r \ll 1 \qquad \tilde{n} = \left(1 + \frac{1}{\beta_r}\right)^{\frac{1}{\Gamma}}$$

$$\Delta T_e = \frac{\pi}{18} T_e \frac{B_r^2 + B_g^2}{B_g^2} \beta_r^{-\frac{2}{\Gamma}} = \frac{\pi}{18} T_e \frac{B_r^2 + B_g^2}{B_g^2} \beta_r^{-\frac{6}{5}}$$

$$\frac{\Delta T_e}{m_i v_A^2} = \frac{\pi}{36} \frac{T_e}{T_i} \frac{B_r^2 + B_g^2}{B_g^2} \beta_r^{\frac{\Gamma-2}{\Gamma}} = \frac{\pi}{36} \frac{T_e}{T_i} \frac{B_r^2 + B_g^2}{B_g^2} \beta_r^{-\frac{1}{5}}$$

Scaling Prediction for Exhaust Heating

Predictions are on the same order as the reported observational scaling, and have a weak dependence on β, which is within the variance of other parameters.

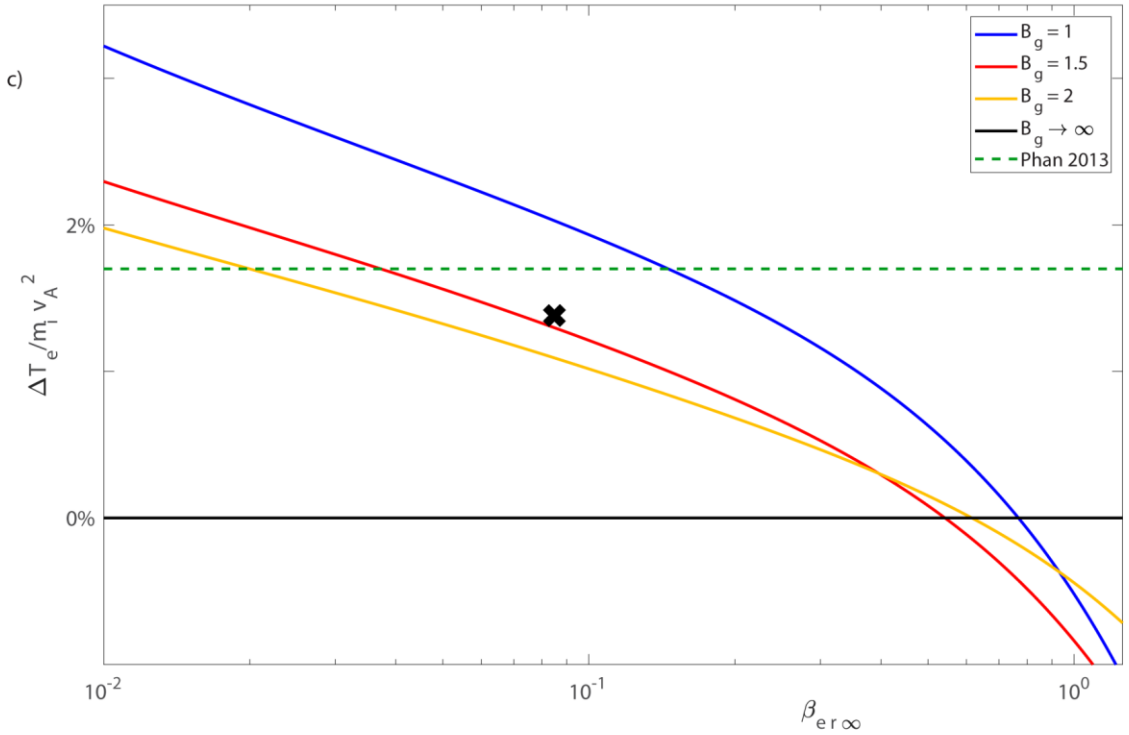

[Wetherton+, GRL, 2019]

Summary of Event Results

- EoS confirmed for a naturally-occurring guide-field reconnection event
- Hybrid simulations with EoS reproduce event well, and model electron heat flux more accurately than reduced mass ratio PIC simulations
- A prediction for how the electron bulk heating scales with upstream parameters in guide-field reconnection was made

Overview

- Drift Kinetics Overview
- Magnetic Reconnection
  - Introduction/Background
  - Description of Anisotropic Model
  - Validating the Model with Spacecraft Data
  - Importance of Mass Ratio in Kinetic Simulations
  - Prediction of Scaling of Electron Heating
- **Drift Kinetic Method for Gradient Estimation in Space Plasma** [Wetherton+, JGR:SP, 2020]
  - Agyrotropy in Magnetized Plasmas
  - Relating Gradients to Agyrotropy
  - Model Derivation/Results
  - Verification on Simulation Data
- Magnetic Mirrors
  - Introduction/Background on Mirrors
  - Overview of the Drift-Kinetic Model
  - Application to Deuterium Device
  - Development of the Sheath Potential
  - Particle-in-Cell Simulations
  - Adding in Sloshing Ion Beams

MMS October 16, 2015 event (Burch et al., 2016)

Crescent distributions were observed in the perpendicular plane for an MMS event. This event is at the magnetopause, where the density varies by a factor of ~15 across the reconnection region.

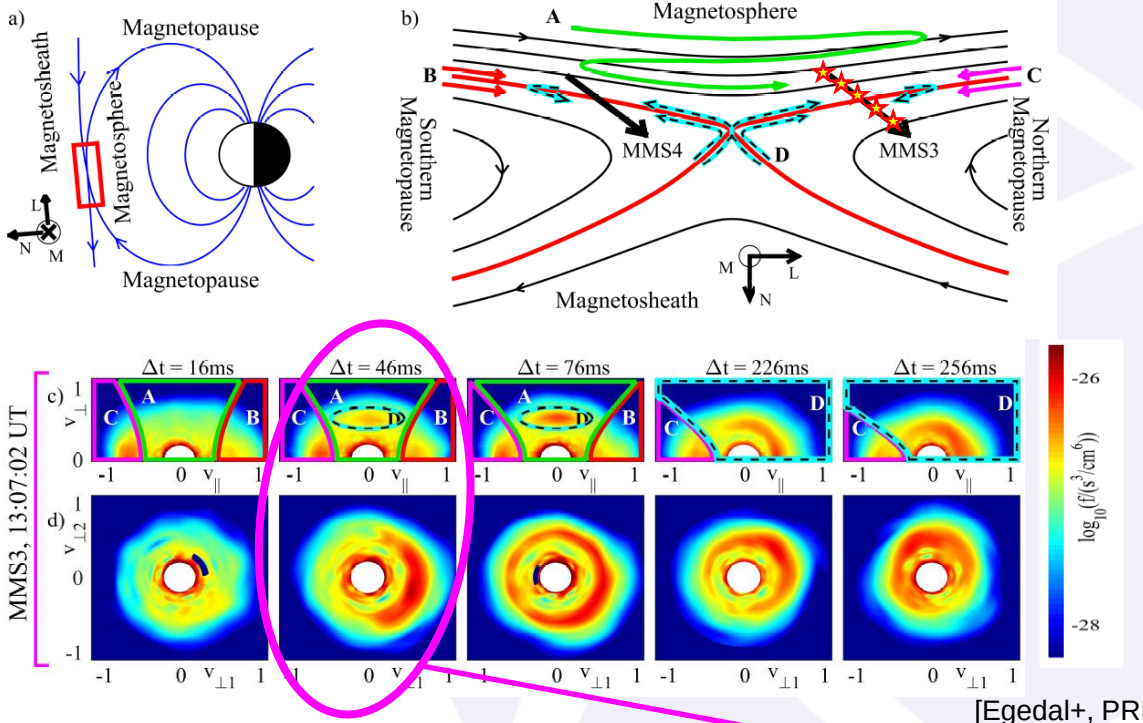

[Egedal+, PRL 2016]

B = 17nT,
Magnetized?

Crescents observed in simulations [Hesse+, 2014]
1D models for cut at x-line [Bessho+, 2016, Shay+, 2016]

Model in Agreement with Kinetic Simulations

Crescent distributions are strongly agyrotropic when binned by electron location, yet when sorted by guiding center location, they are gyrotropic rings in the perpendicular plane.

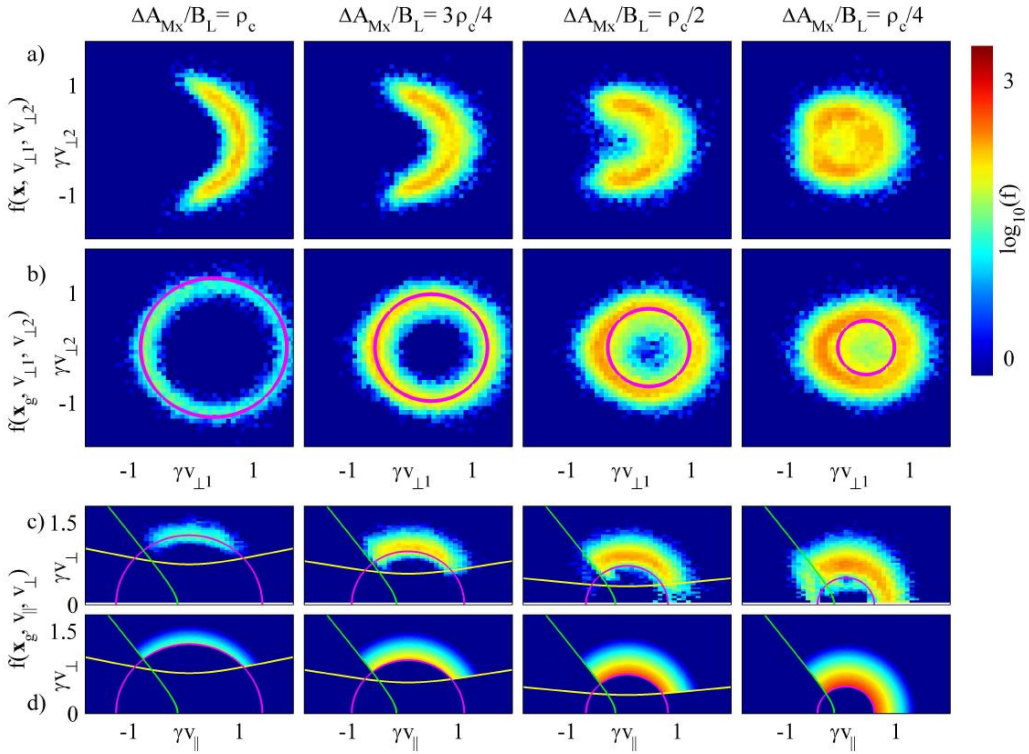

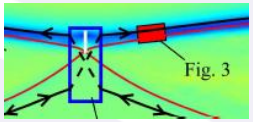

$$f(\mathbf{x}, \mathbf{v})$$

$$f_g(\mathbf{x}_g, \mathbf{v}) \equiv f(\mathbf{x}_g - \boldsymbol{\rho}, \mathbf{v})$$

$$\boldsymbol{\rho}(\phi) = m\mathbf{v}\times\mathbf{B}/(qB^2)$$

$$f_{g\perp}(\mathbf{x}_g, \mathbf{v}_\perp) = \int f_g(\mathbf{x}_g, \mathbf{v})\, dv_\parallel$$

$$\bar{f}_g(v_\parallel, v_\perp)$$

$$\bar{f}_g \simeq f_{xline}(\mathcal{E} - q\Phi_N)\, H(\mathcal{E} - \mathcal{E}_X)\, H(\mathcal{E}_\perp - \mathcal{E}_{X\perp})$$

[Egedal+, PRL 2016]

Measures of Agyrotropy in simple gradient model

- Simple drift-kinetic equilibrium with gradient and the apparent agyrotropy

$$\bar{f} = \left(\frac{m}{2\pi T}\right)^{3/2} n_0 \left(1 + \frac{x}{L_\Delta}\right) e^{-\frac{m|v|^2}{2T}} \qquad f = \bar{f}(\boldsymbol{x} - \boldsymbol{\rho}) \qquad \xi = \rho_{th}/L_\Delta$$

Various proposed measures of agyrotropy are shown under varying gradient strength.

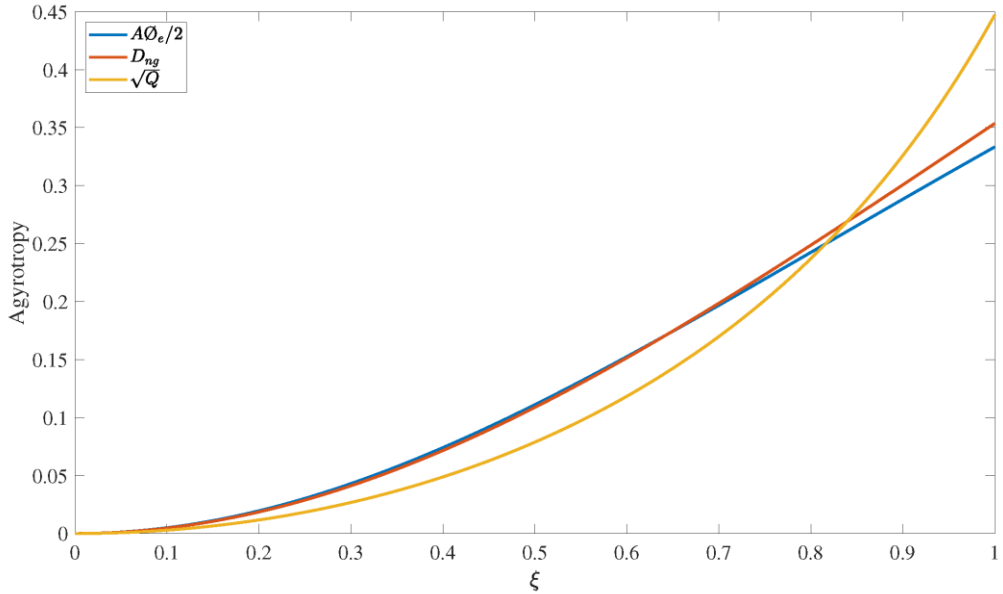

[Wetherton+, JGR:SP, 2020]

Gradient illustration

Gradients in the guiding center distribution are reflected in an asymmetry in the distribution measured in the $\boldsymbol{\nabla \bar{f} \times B}$ direction.

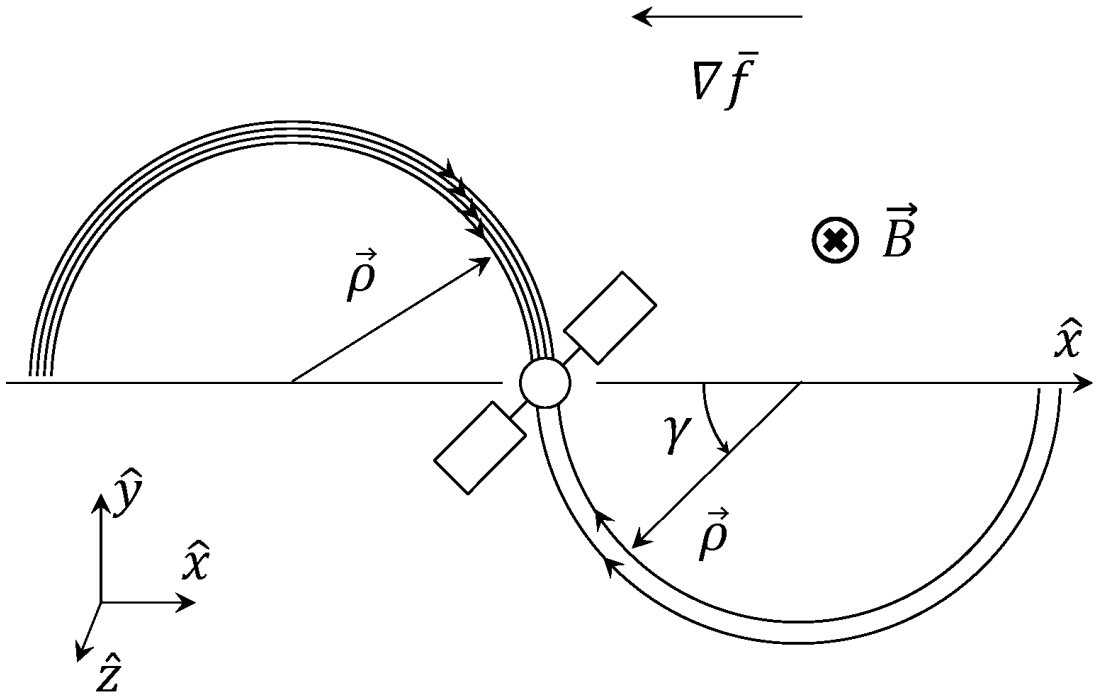

[Wetherton+, JGR:SP, 2020]

Drift Kinetic Perturbations: Basic Equations

$$\bar{f} = \frac{1}{2\pi}\int f \mathrm{d}\gamma$$

$$\tilde{f} = f - \bar{f}$$

$$\tilde{f}(\mathbf{x}, U, \mu, \gamma, t) = \boldsymbol{\rho}\cdot\left[q\frac{\partial \mathbf{A}}{\partial t}\frac{\partial \bar{f}}{\partial U} - q\left(\mathbf{b}\times\mathbf{v}_D\right)\frac{\partial \bar{f}}{\partial \mu} - \boldsymbol{\nabla}\bar{f}\right] + \frac{v_\parallel \mu}{\Omega_s}\frac{\partial \bar{f}}{\partial \mu}\left(\hat{\boldsymbol{\rho}}\hat{\mathbf{v}}_\perp : \boldsymbol{\nabla}\mathbf{b} - \frac{1}{2}\mathbf{b}\cdot\boldsymbol{\nabla}\times\mathbf{b}\right)$$

$$\mathbf{v}_D = \frac{\mathbf{E}\times\mathbf{B}}{B^2} - \frac{1}{\Omega_e}\mathbf{b}\times\left(\frac{\mu}{m}\boldsymbol{\nabla}B + v_\parallel^2(\mathbf{b}\cdot\boldsymbol{\nabla})\mathbf{b} + v_\parallel\frac{\partial \mathbf{b}}{\partial t}\right)$$

$$\boldsymbol{\nabla}_{U,\mu} = \boldsymbol{\nabla}_{v_\parallel, v_\perp} - \boldsymbol{\nabla}\mu\frac{\partial}{\partial \mu} - \boldsymbol{\nabla}U\frac{\partial}{\partial U}$$

Drift Kinetic Model Results

$$\nabla_\perp \bar{f} = e\mathbf{E}_\perp \frac{\partial \bar{f}}{\partial \mathcal{E}} + e\left(\mathbf{b}\times\mathbf{v}_D\right)\frac{\partial \bar{f}}{\partial \mu} - \frac{1}{\pi\rho^2}\int_0^{2\pi} \boldsymbol{\rho} f \,\mathrm{d}\gamma$$

$$\mathcal{M}_{k,l} = \int v_\perp^k v_\parallel^l \bar{f}\,\mathrm{d}^3 v$$

$$\begin{aligned}\nabla_\perp \mathcal{M}_{k,l} = -2\Omega_e \int \hat{\boldsymbol{\rho}}_e v_\parallel^l v_\perp^{k-1} f \,\mathrm{d}^3 v - \frac{2\pi e \mathbf{E}_\perp}{m}\left[\delta_{k0}\int v_\parallel^l \bar{f}_\parallel \mathrm{d}v_\parallel + k\int v_\parallel^l v_\perp^{k-1}\bar{f}\,\mathrm{d}v_\perp \mathrm{d}v_\parallel\right] \\ + (\mathbf{b}\cdot\nabla)\mathbf{b}\left[(l+1)\mathcal{M}_{k,l} - 2\pi\left(\delta_{k0}\int v_\parallel^{l+2}\bar{f}_\parallel \mathrm{d}v_\parallel + k\int v_\parallel^{l+2} v_\perp^{k-1}\bar{f}\,\mathrm{d}v_\perp \mathrm{d}v_\parallel\right)\right] \\ + \frac{\partial \mathbf{b}}{\partial t}\left[l\mathcal{M}_{k,l-1} - 2\pi\left(\delta_{k0}\int v_\parallel^{l+1}\bar{f}_\parallel \mathrm{d}v_\parallel + k\int v_\parallel^{l+1} v_\perp^{k-1}\bar{f}\,\mathrm{d}v_\perp \mathrm{d}v_\parallel\right)\right]\end{aligned}$$

Drift Kinetic Model Moments

$$n = \mathcal{M}_{0,0}$$

$$p_\perp = \frac{m}{2}\mathcal{M}_{2,0}$$

$$\nabla_\perp n = -\frac{2\pi e \mathbf{E}_\perp}{m}\int \bar{f}_\parallel \mathrm{d}v_\parallel + (\mathbf{b}\cdot\nabla)\mathbf{b}\left(n - 2\pi\int v_\parallel^2 \bar{f}_\parallel \mathrm{d}v_\parallel\right) - \frac{\partial \mathbf{b}}{\partial t}\left(2\pi\int v_\parallel \bar{f}_\parallel \mathrm{d}v_\parallel\right) - \int \frac{\boldsymbol{\rho}_e f}{\rho_e^2}\mathrm{d}^3 v$$

$$\nabla_\perp p_\perp = -ne\left(\mathbf{E}_\perp + \mathbf{u}_e \times \mathbf{B}\right) - mnu_\parallel \frac{\partial \mathbf{b}}{\partial t} + (\mathbf{b}\cdot\nabla)\mathbf{b}\left(mnu_\parallel^2 + p_\perp - p_\parallel\right)$$

Density gradients

$$\nabla_\perp n = -\frac{2\pi e \mathbf{E}_\perp}{m}\int \bar{f}_\parallel \mathrm{d}v_\parallel + (\mathbf{b}\cdot\nabla)\mathbf{b}\left(n - 2\pi\int v_\parallel^2 \bar{f}_\parallel \mathrm{d}v_\parallel\right) - \frac{\partial \mathbf{b}}{\partial t}\left(2\pi\int v_\parallel \bar{f}_\parallel \mathrm{d}v_\parallel\right) - \int \frac{\boldsymbol{\rho}_e f}{\rho_e^2}\mathrm{d}^3 v$$

Density gradients match when calculated with the DK method from particle data and from finite difference on fluid moments, albeit with some noise.

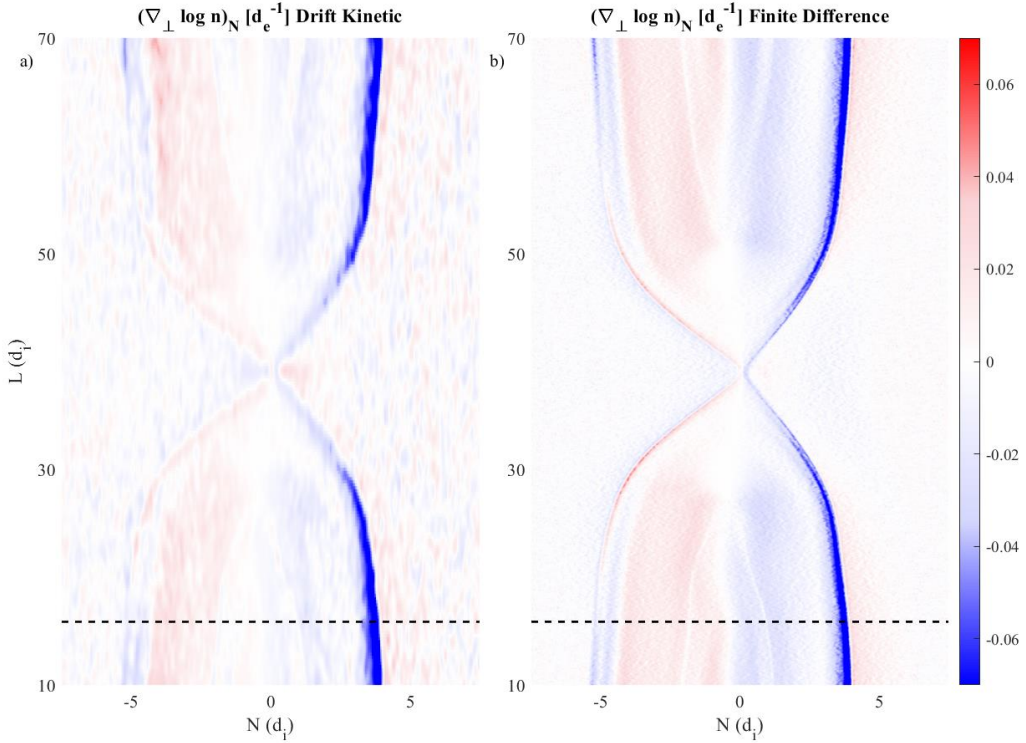

[Wetherton+, JGR:SP, 2020]

Perpendicular pressure gradients

Perpendicular pressure gradients reduce to local fluid quantities with the DK method. The local measure generally corresponds to finite difference calculations.

$$\nabla_\perp p_\perp = -ne\left(\mathbf{E}_\perp + \mathbf{u}_e \times \mathbf{B}\right) - mnu_\parallel \frac{\partial \mathbf{b}}{\partial t} + (\mathbf{b}\cdot\nabla)\mathbf{b}\left(mnu_\parallel^2 + p_\perp - p_\parallel\right)$$

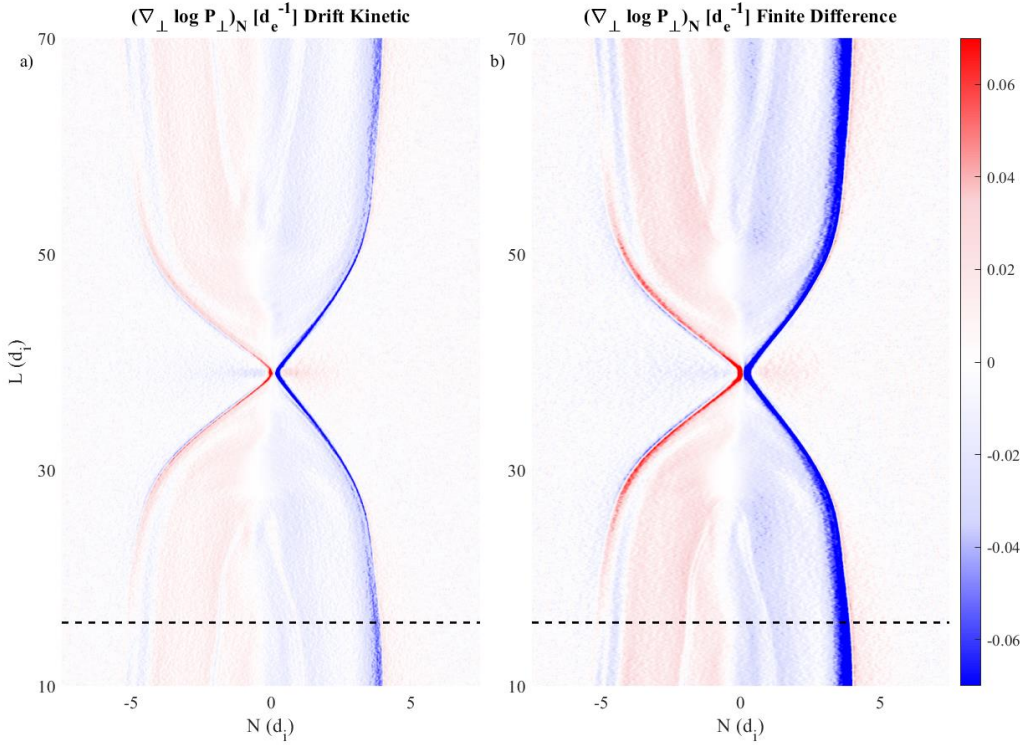

[Wetherton+, JGR:SP, 2020]

Density gradient cuts

$$\nabla_\perp n = -\frac{2\pi e \mathbf{E}_\perp}{m}\int \bar{f}_\parallel \mathrm{d}v_\parallel + (\mathbf{b}\cdot\nabla)\mathbf{b}\left(n - 2\pi\int v_\parallel^2 \bar{f}_\parallel \mathrm{d}v_\parallel\right) - \frac{\partial \mathbf{b}}{\partial t}\left(2\pi\int v_\parallel \bar{f}_\parallel \mathrm{d}v_\parallel\right) - \int \frac{\boldsymbol{\rho}_e f}{\rho_e^2}\mathrm{d}^3 v$$

Density gradients along a cut can be seen to match trends well for simulations with different levels of asymmetry, though with noise. Some accuracy is lost for the strongest jumps in the most asymmetric simulation.

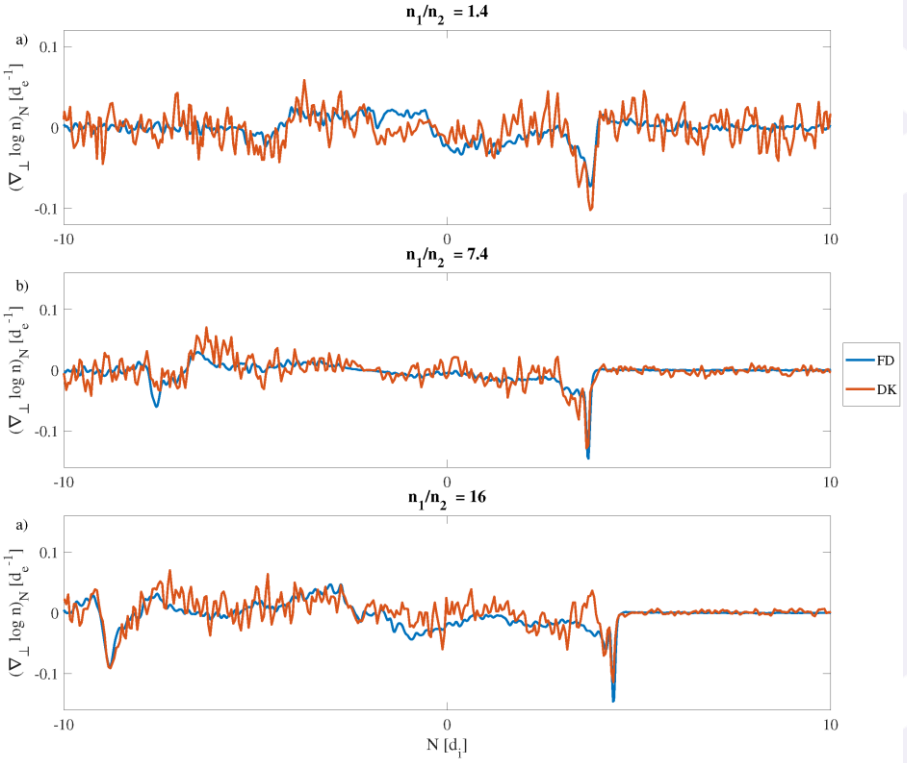

[Wetherton+, JGR:SP, 2020]

Conclusions

- Gradients are inherently linked to agyrotropy, and this allows for prediction of gradients from single-point measurements.
- A drift kinetic model is developed to predict gradients from only local data.
- The model is validated with data from fully-kinetic simulations.
- This could be useful to spacecraft missions with distribution diagnostics, especially single spacecraft missions and those where gradient scales are smaller than the separation between spacecraft.

Overview

- Drift Kinetics Overview
- Magnetic Reconnection
  - Introduction/Background
  - Description of Anisotropic Model
  - Validating the Model with Spacecraft Data
  - Importance of Mass Ratio in Kinetic Simulations
  - Prediction of Scaling of Electron Heating
- Drift Kinetic Method for Gradient Estimation in Space Plasma
  - Agyrotropy in Magnetized Plasmas
  - Relating Gradients to Agyrotropy
  - Model Derivation/Results
  - Verification on Simulation Data
- **Magnetic Mirrors** [Wetherton+,PoP, 2021]
  - Introduction/Background on Mirrors
  - Overview of the Drift-Kinetic Model
  - Application to Deuterium Device
  - Development of the Sheath Potential
  - Particle-in-Cell Simulations
  - Adding in Sloshing Ion Beams

Background- Magnetic Mirrors

- Magnetic mirrors confine charged particles via the mirror force on magnetized particles
- The mirror contains a central region with B strong enough to remain magnetized and confined with end regions of stronger B to reflect particles inward
- Particles travelling nearly parallel to the magnetic field lines will not be confined by the mirror, making the device inherently lossy.

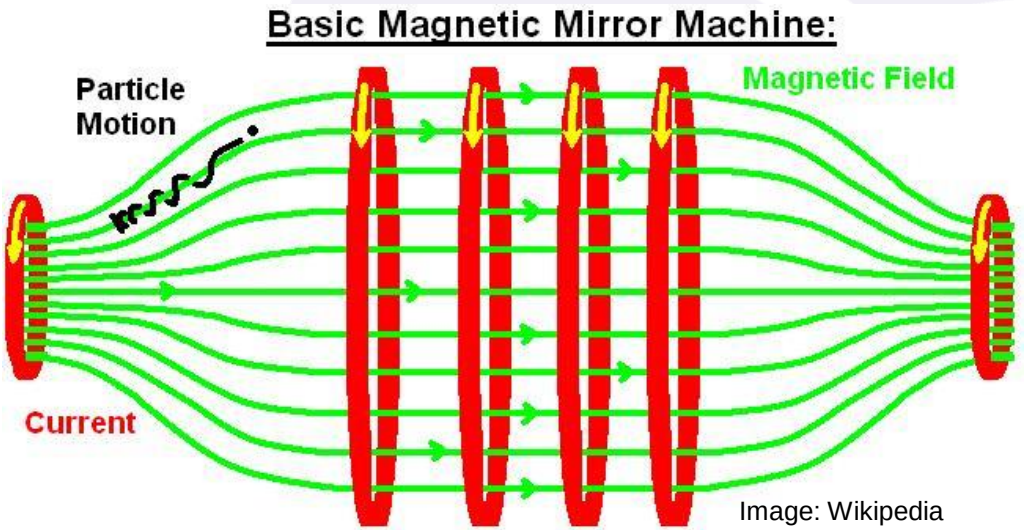

Image: Wikipedia

The Loss Cone

- Confinement depends on being able to achieve large values of B_m/B_0, but B_0 must be large enough to maintain magnetization of the fastest ions in the central region.
- Being able to maintain large magnetic fields is important.

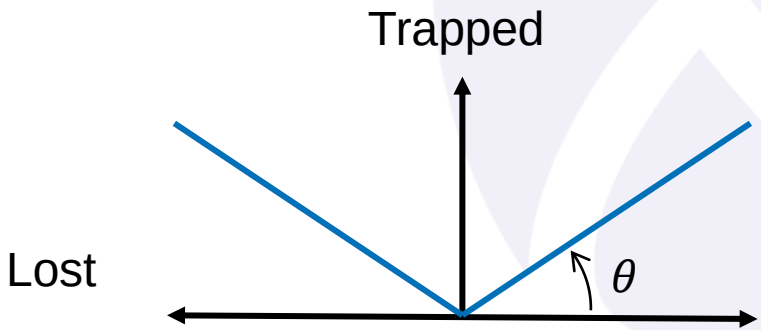

$$\theta = \tan^{-1}\left(\frac{1}{\sqrt{B_m/B_0 - 1}}\right)$$

Issues with mirrors

- End losses lead to poor electron confinement
- The simple mirror is unstable to MHD interchange modes
- Several approaches exist to address this, but they were often complicated and mirrors fell out of favor in the US
- Russians continued work with mirrors
- The Gas Dynamic Trap (GDT) approach can address many of the issues
- GDT exploits pressure weighted curvature to stabilize to MHD interchange
- The internal solenoidal cell is collisional for trapped ions, while outflows into the expander are supersonic

Motivation

- Recent advances on magnetic mirrors have made them an attractive fusion concept once again.
- GDT in Novosibirsk, particularly gives encouraging results (stability, confinement of thermal electrons, etc.).
- We will look at the physics of end losses and confinement in a GDT-like expander region.

Basic device layout

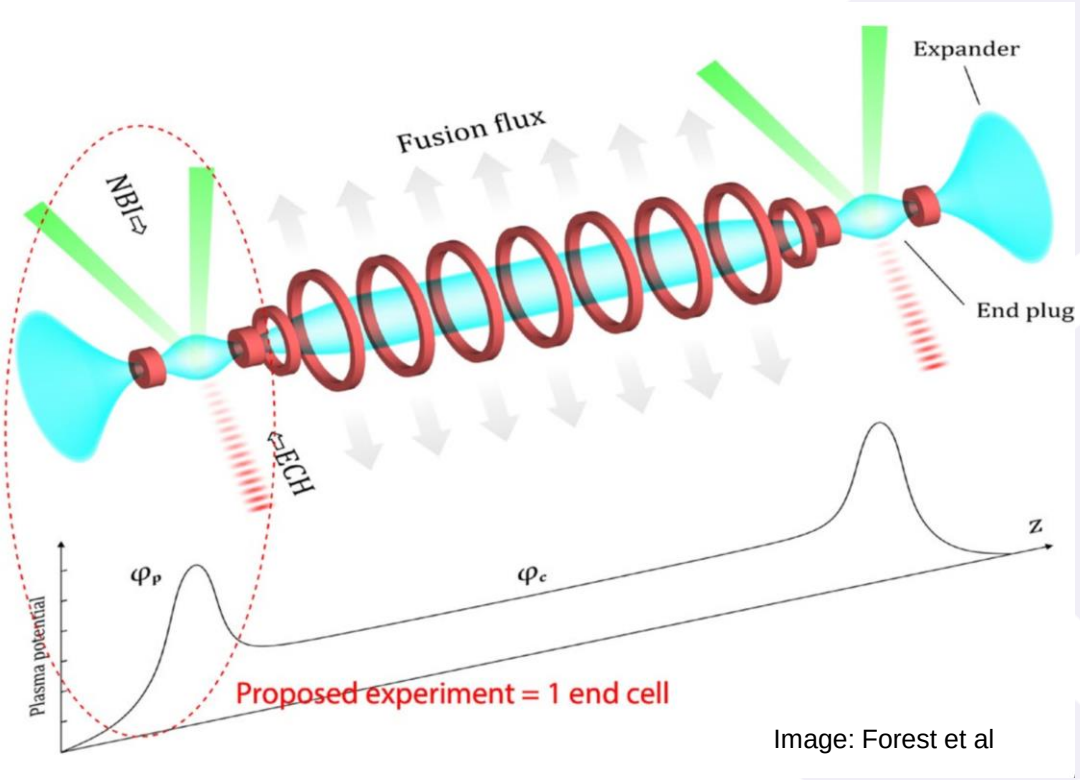

Image: Forest et al

Model Basis- Types of Orbits

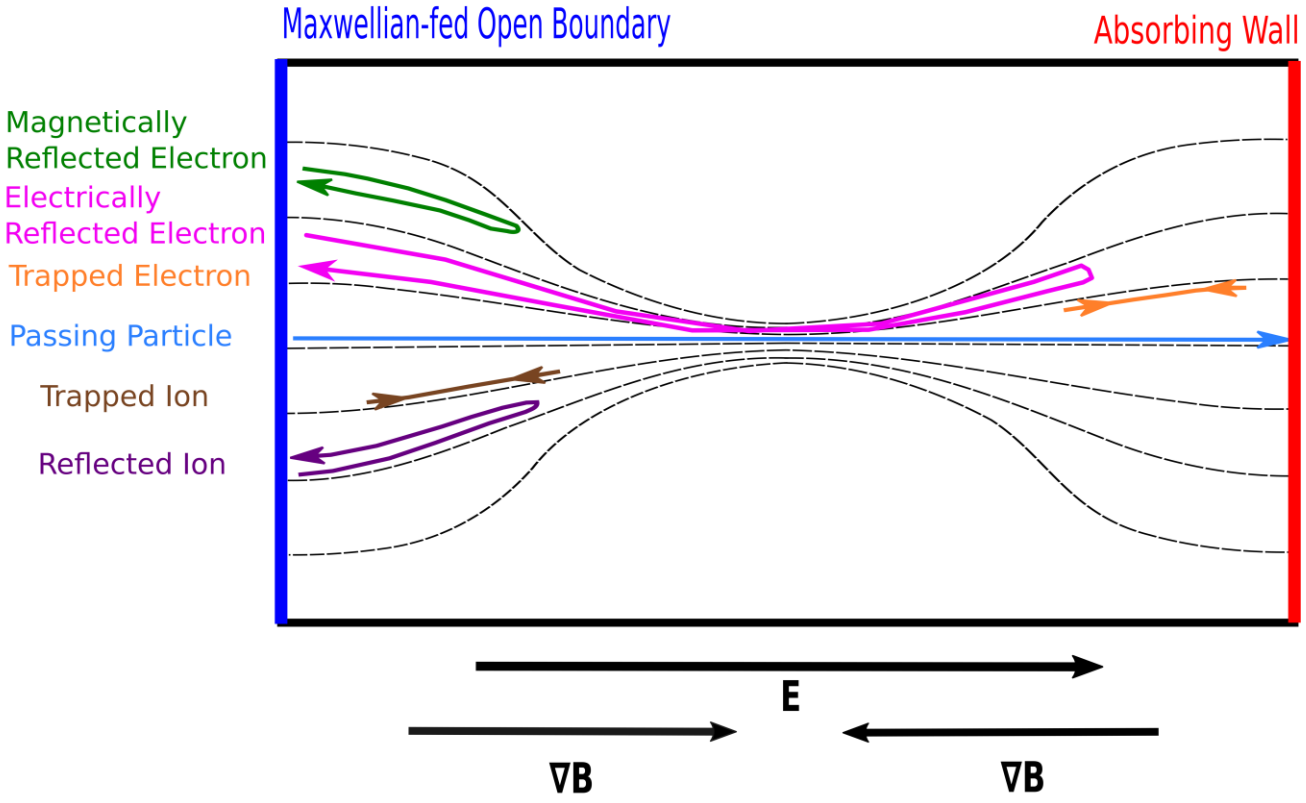

[Wetherton+, PoP, 2021]

Model- Classifying Orbits by 1D profiles

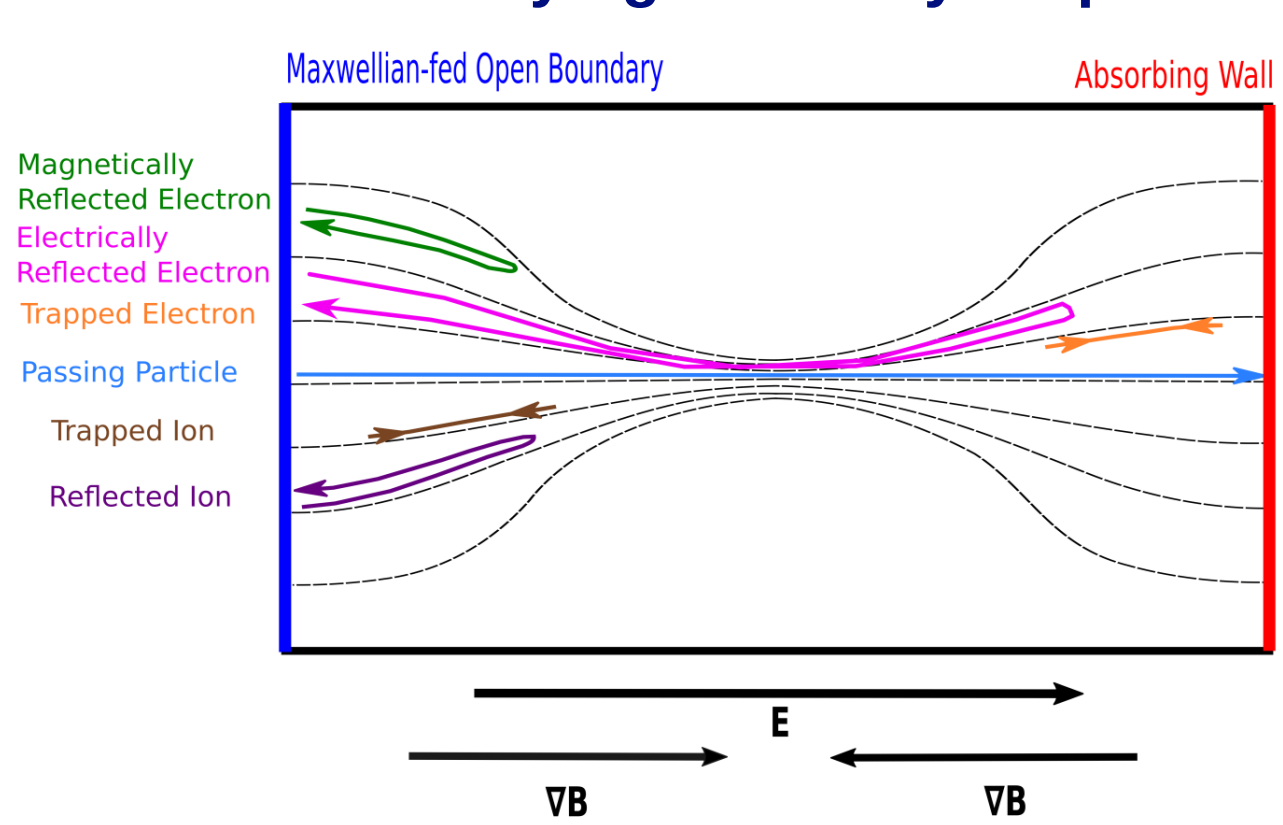

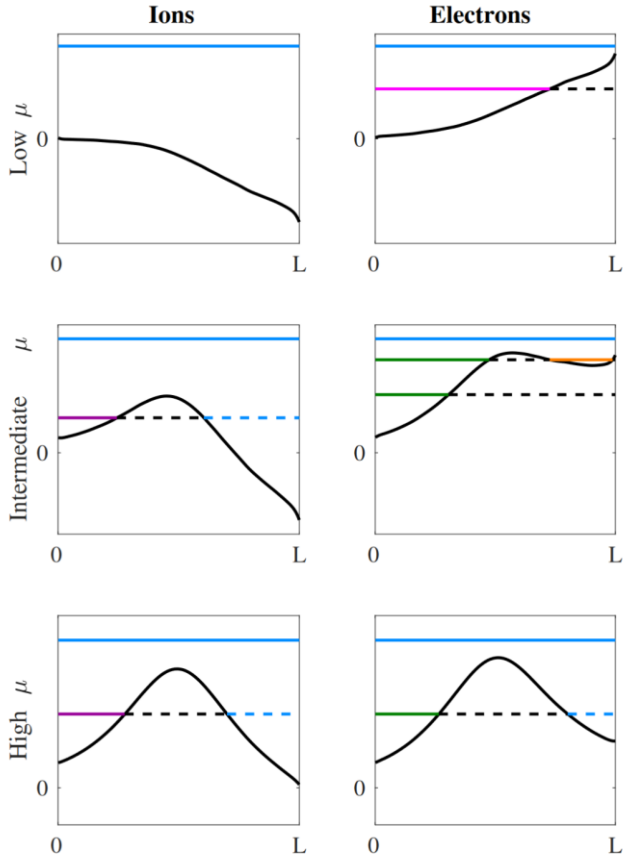

[Wetherton+, PoP, 2021]

Distribution Function Mapping

- Given the 1D profile of the ambipolar potential and magnetic field strength for a given flux tube, we can assign all of phase space to an orbit type.
- Assuming an isotropic upstream distribution function, we assign the value through Liouville's theorem as shown.
- Distributions at any point can be calculated as such with given profiles.

$$f(\mathbf{x},\mathbf{v}) = \begin{cases} \xi_t f_\infty(\mathcal{E} + q\phi_{||}) & \text{trapped} \\ f_\infty(\mathcal{E} + q\phi_{||}) & \text{passing}+ \\ f_\infty(\mathcal{E} + q\phi_{||}) & \text{reflected} \\ 0 & \text{passing}- \\ 0 & \text{blocked} \end{cases}$$

Iterating for the Potential Profile

- While the background magnetic field strength profile should be relatively unchanged, we have no a priori form for the ambipolar parallel potential.
- As such, we apply an iterative approach that adjusts the potential profile such that the model achieves quasineutrality at each point.
- We can start with any reasonable initial potential guess (including zero) and update the potential through the following equations:

$$\phi_{||}^{k+1}(x) = \phi_{||}^{k}(x) + \lambda \Delta\phi_{||}^{k}(x)$$

$$\Delta\phi_{||}^{k}(x) = \frac{T_e T_i}{e(T_e + T_i)} \ln\left(\frac{n_i^k(x)}{n_e^k(x)}\right)$$

- The iteration is based on a Boltzmann response for both species, which is a crude approximation, but it converges on quasineutrality nonetheless.

Application to Deuterium Device, Bm/Bo = 30

- Mirror field is symmetric
- Ambipolar potential ~-5 Te develops
- Potential jump in sheath ~ Te/2
- Ion bulk flow supersonic past throat
- Electrons roughly isothermal to the left, become anisotropic in expander
- Ion temperature much smaller in expander

[Wetherton+, PoP, 2021]

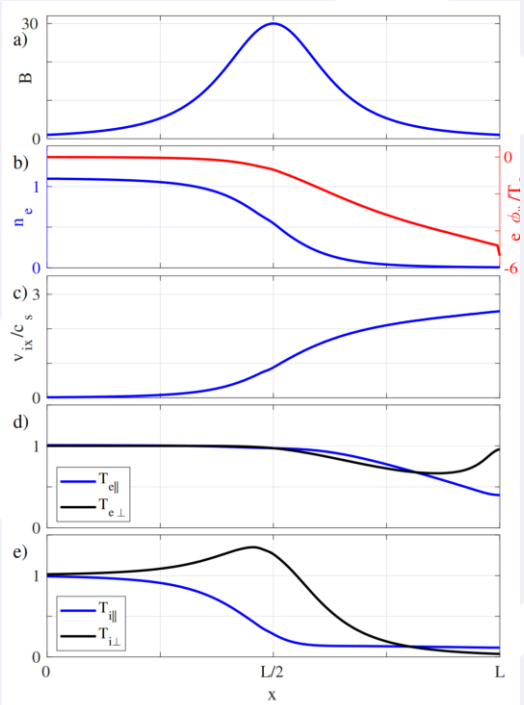

Boundary Conditions- The Sheath Potential

- In steady-state, to maintain quasineutrality, the electron and ion fluxes to the wall must be equal.
- We account for this with a boundary value for the potential at the wall; the discontinuity represents a plasma sheath where the potential varies sharply within the space of about a Debye length from the absorbing wall.
- We also iterate this to ensure the ion and electron fluxes to the absorbing wall are equal.

VPIC Simulations

- We ran several 2D fully-kinetic VPIC simulations.
- This one has parameters:

$$\frac{m_i}{m_e} = 400,\ \frac{B_m}{B_0} = 5,\ \beta_e = 0.03,\ \frac{\omega_{pe}}{\omega_{ce}} = 1.22$$

$$L_x \times L_z = 200\ d_e \times 100\ d_e$$

- Density and ion bulk x velocity shown

[Wetherton+, PoP, 2021]

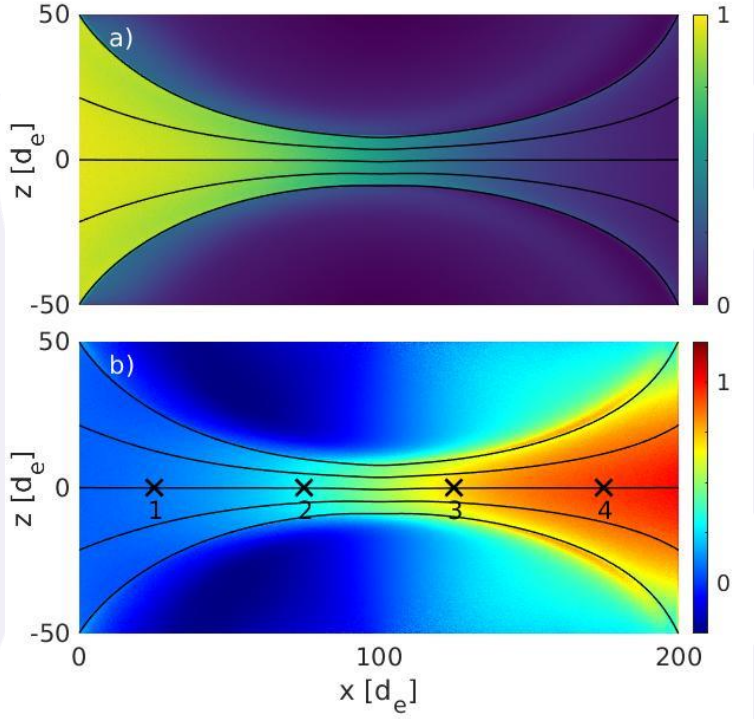

Electron Distributions- VPIC and Model

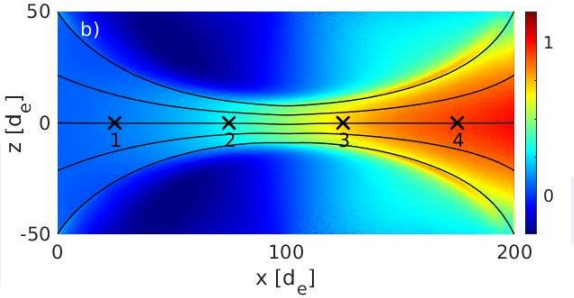

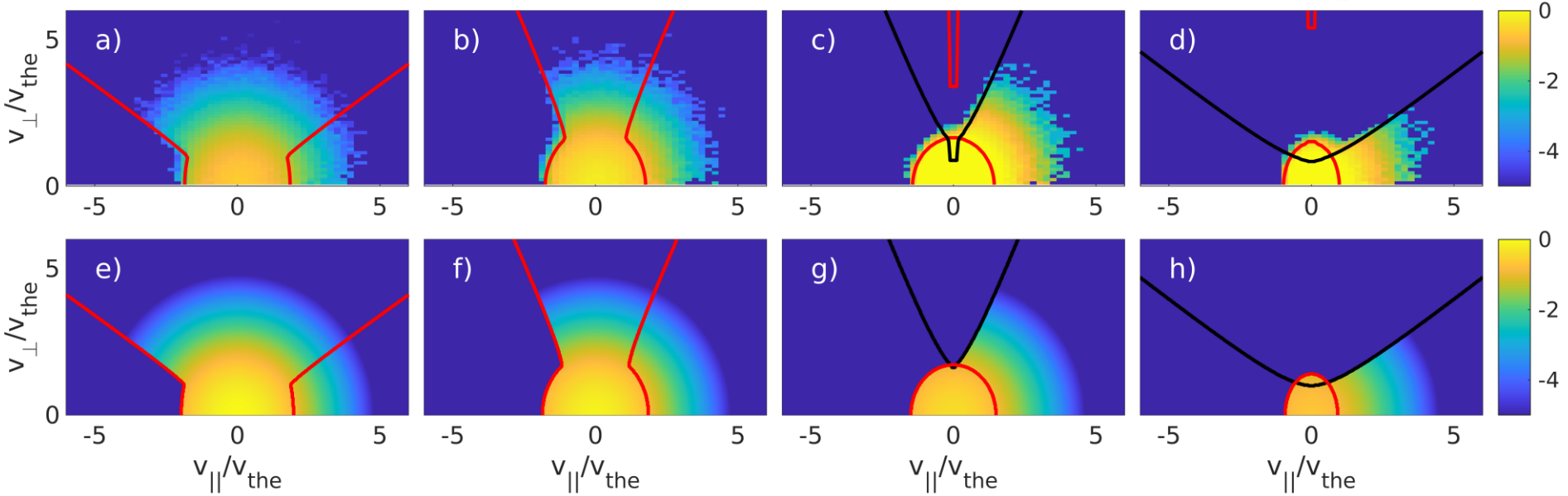

[Wetherton+, PoP, 2021]

Ion Distributions- VPIC and model

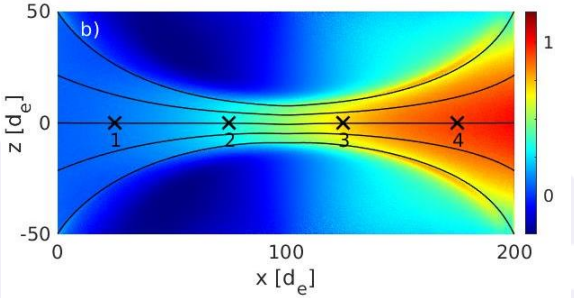

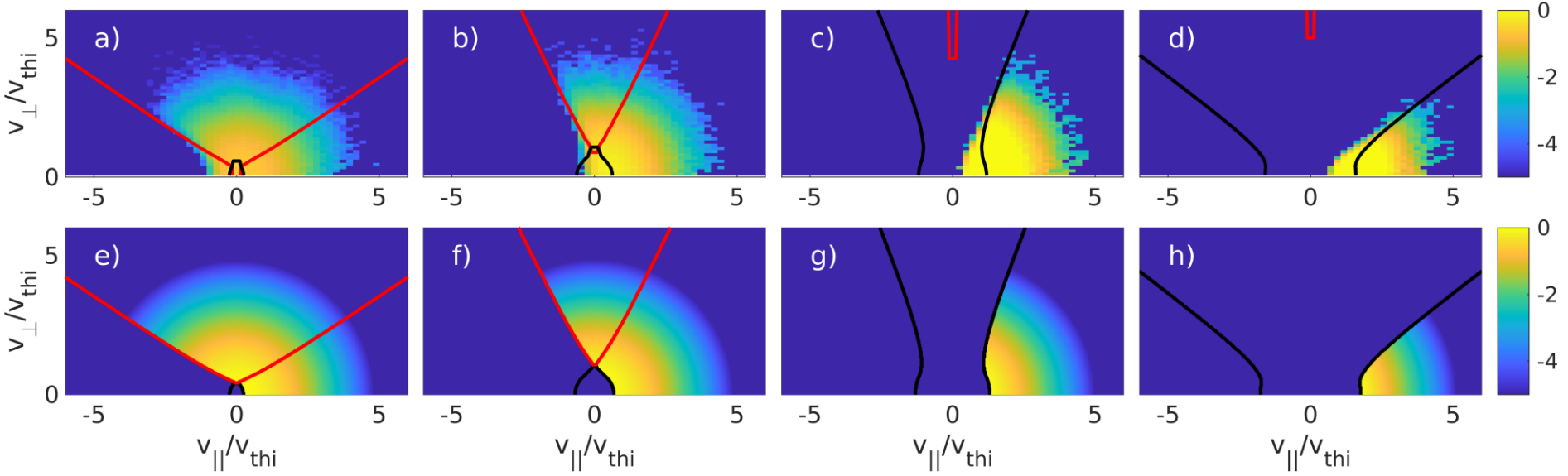

[Wetherton+, PoP, 2021]

Adding in Sloshing Ion Beams

- Simulation is same as last, but with a beam ion population added.
- Beam parameters:

$$\frac{n_b}{n_0} = 0.03,\ E_b = 20\ T_{i0}, \theta_b \approx 18.4°$$

- Electron, background ion, and beam ion density plotted.

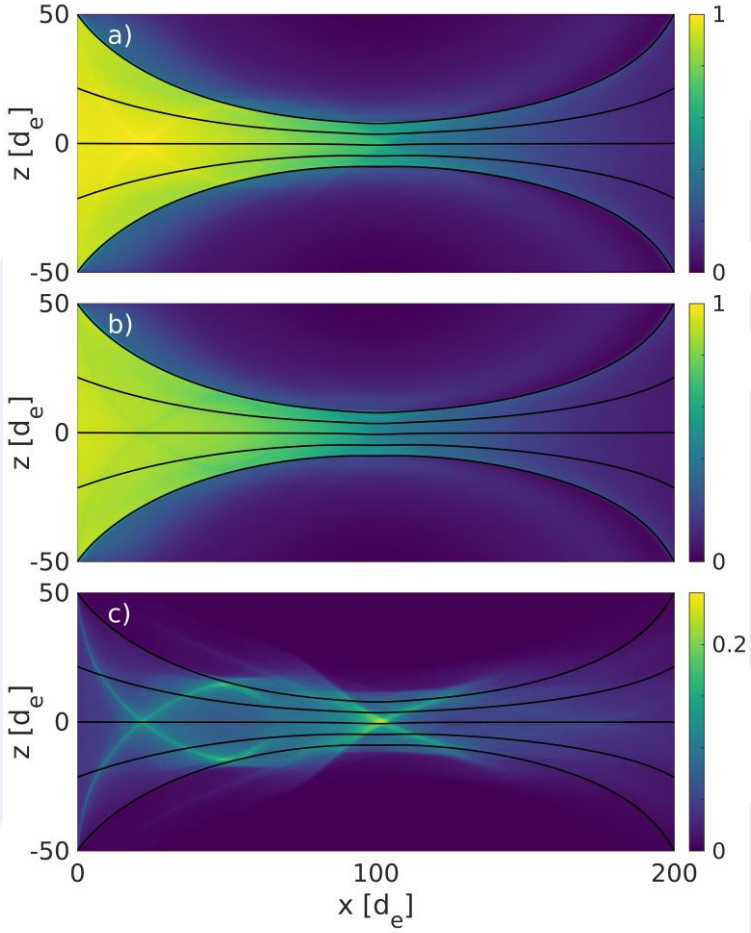

[Wetherton+, PoP, 2021]

Adjusting the Iterative Scheme to Include Beam Ions

- We treat the density profile of the beam ions as a given (taken from the VPIC data here).
- The quasineutrality condition updates slightly, assuming the background ions and electrons have Boltzmann responses.
- The approximate equation below is derived for equal electron and ion temperatures with the temperature scaling from the beamless case reinserted.

$$\Delta\phi_{||}^{k}(x) = \frac{2T_eT_i}{e(T_e+T_i)} \ln\left(\frac{n_b(x) + \sqrt{n_b(x)^2 + 4n_e^k(x)n_i^k(x)}}{2n_e^k(x)}\right)$$

Field Line Profile Comparison

- The model can also reproduce profiles wi
  lower quality at peak beam density

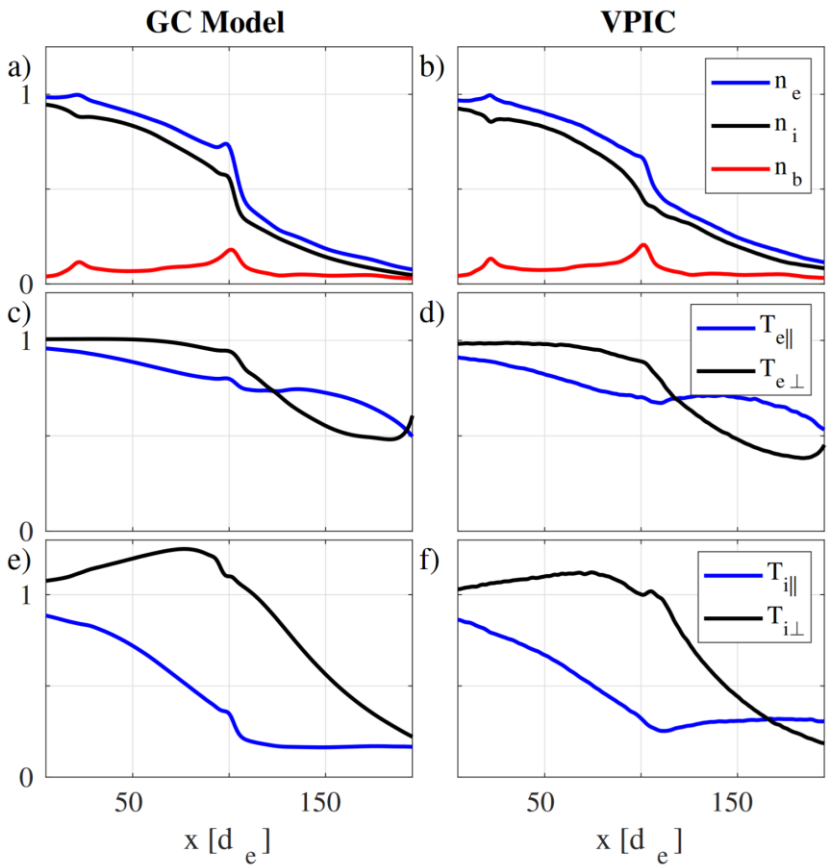

[Wetherton+, PoP, 2021]

Ambipolar Potential with Beam

- Electron density is enhanced in region
- This corresponds to an altered profile
- The sheath potential does not seem to

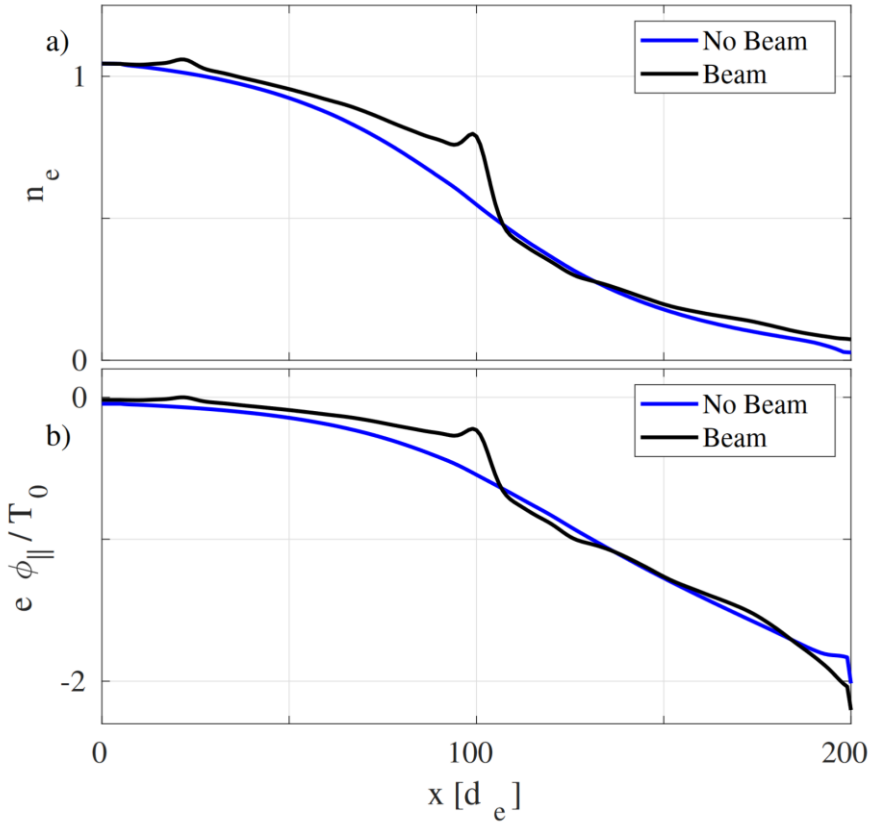

[Wetherton+, PoP, 2021]

Discussion/Conclusion

- The expander region of a magnetic mirror is well-described by a drift-kinetic model that relates orbit types to upstream distribution conditions through Liouville's theorem.
- An ambipolar potential develops, which the model finds through the quasineutrality condition. This forms a built-in thermal barrier for electrons.
- Simulations confirm the form of the ion and electron distributions and fluid profiles.
- The effects of sloshing ion beams are incorporated into the model.

Questions?

Physics governing the structure of guide-field reconnection

- The reconnecting electric field aligns with the guide field
- Naively, this accelerates electrons along field lines
- Quasineutrality requires an in-plane potential to develop to counter this
- The combination of the two governs parallel energization
- In-plane E creates polarization currents for ions
- With density continuity and flux conservation, this generates a quadrupolar density perturbation

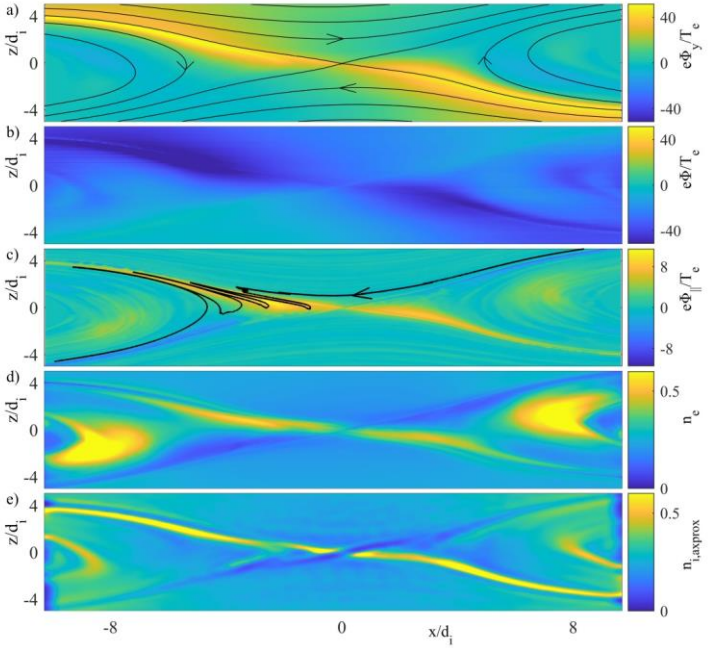

[Wetherton+,JGR:SP, 2021]

Compressing Case

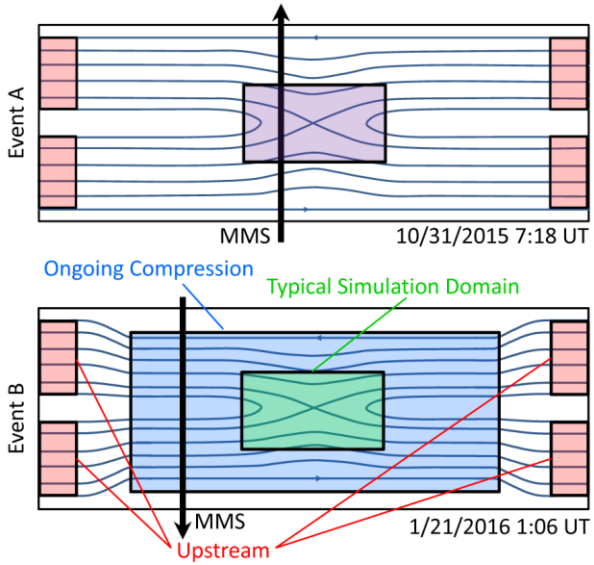

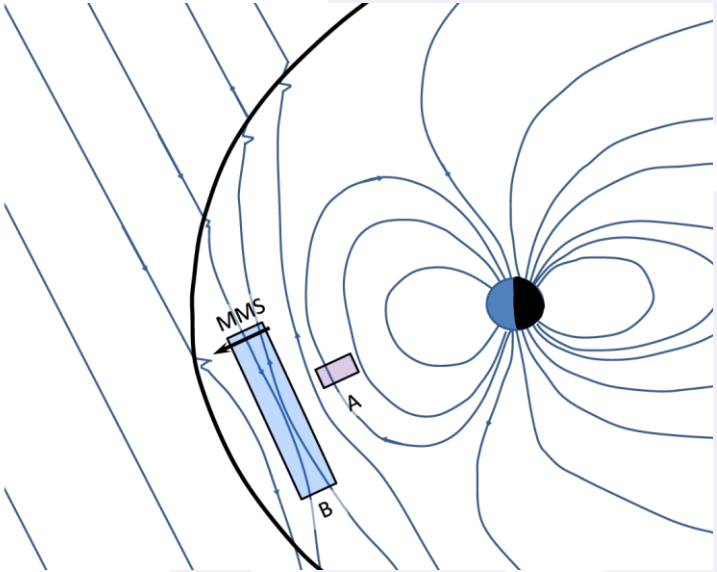

[Wetherton+,JGR:SP, 2021]

Model Tested Against Eastwood Event

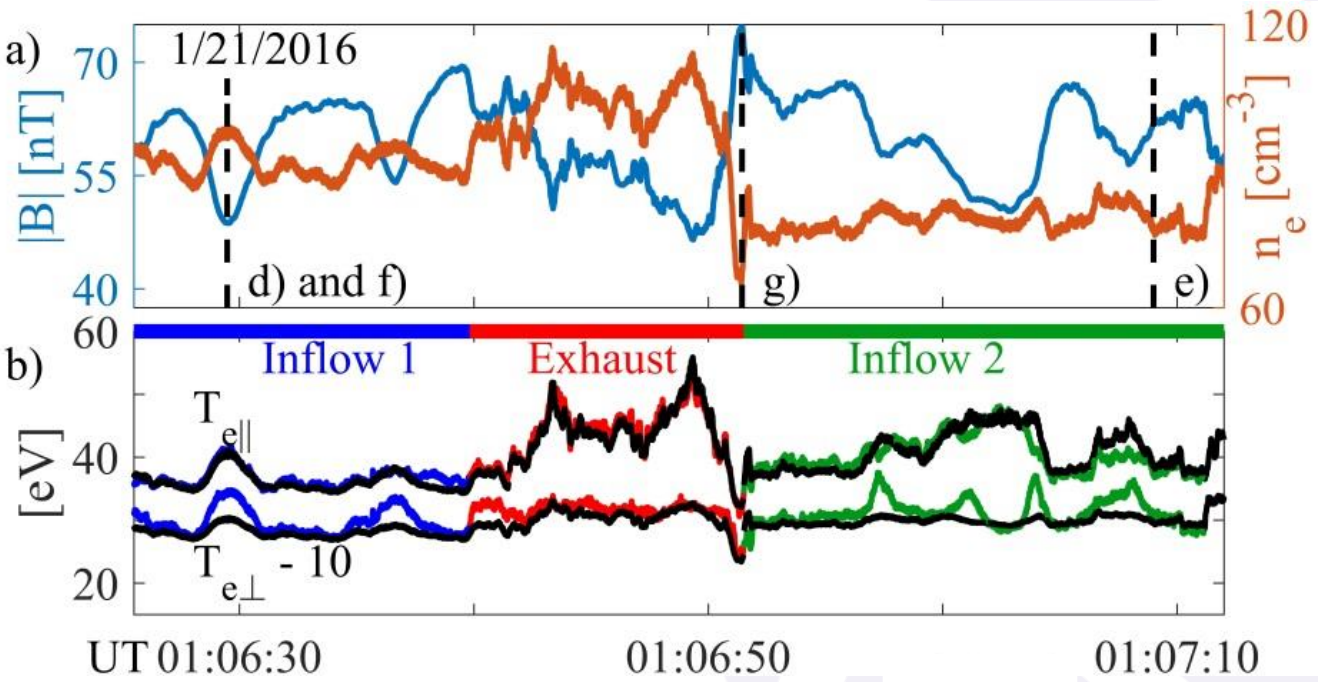

[Wetherton+,JGR:SP, 2021]

Compressing Flux Tube

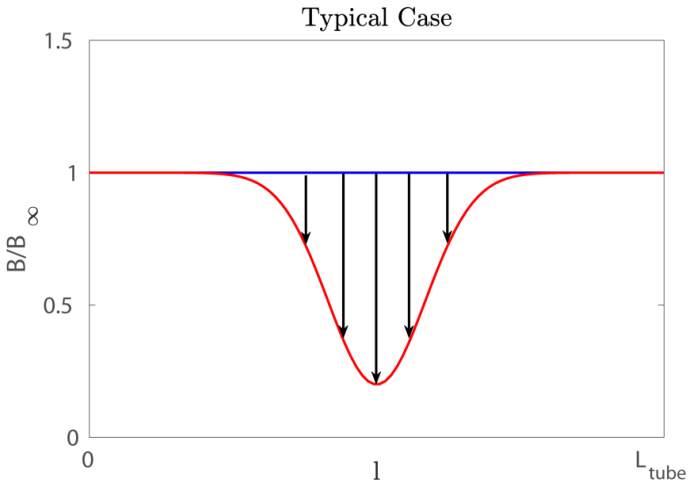

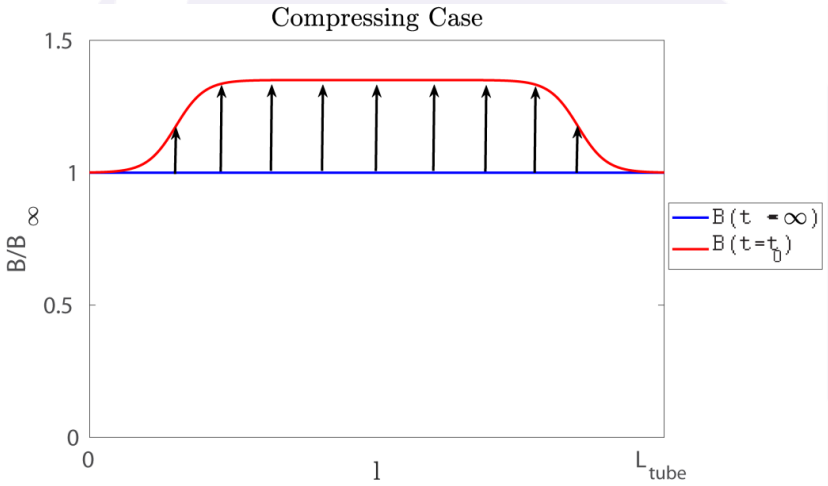

[Wetherton+,JGR:SP, 2021]

Comparing Events

[Wetherton+,JGR:SP, 2021]

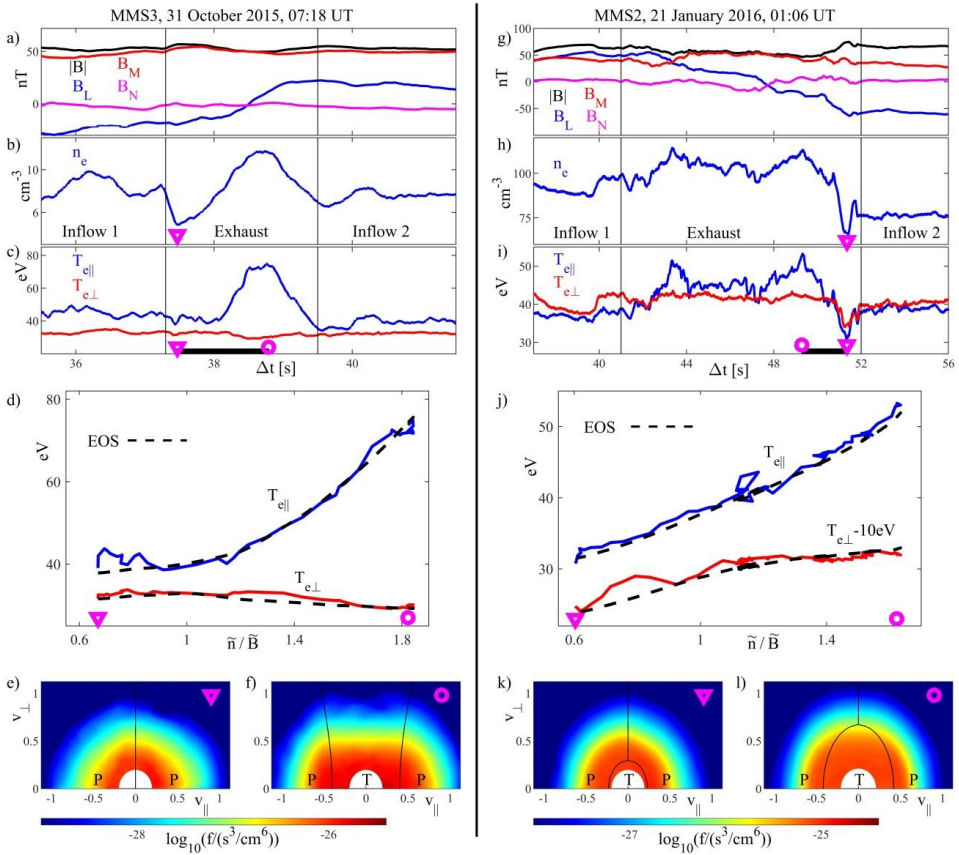

Upstream Parameters set by TP Boundary

[Wetherton+,JGR:SP, 2021]

- Trapped-passing boundaries can be inferred from a discontinuity in the distribution function
- The closed curve shape of the TP boundary can only come from $\phi_{||} > 0$ and $B > B_\infty$.
- This is consistent with the observed isotropic cooling in the cavity.

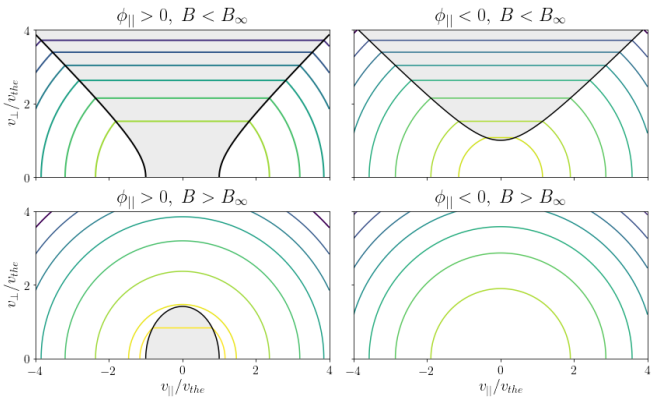

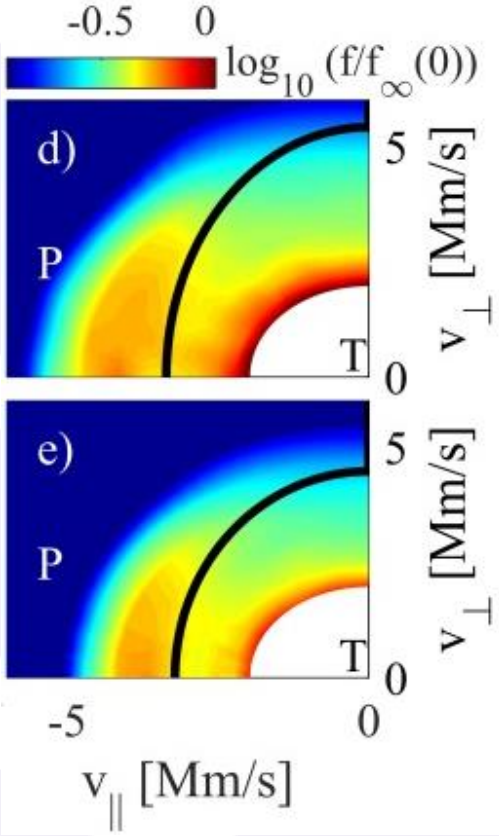

Eastwood Event MMS Observations

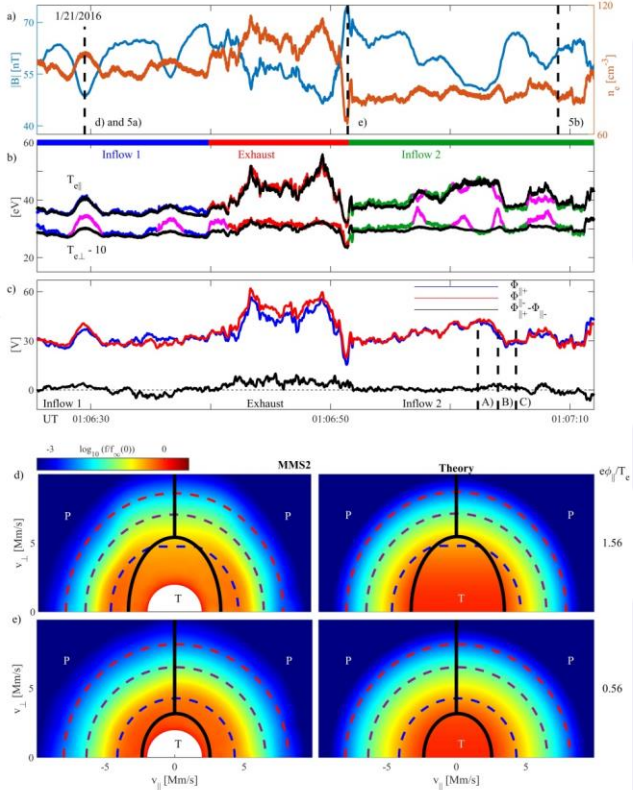

[Wetherton+,JGR:SP, 2021]

Scalings of Three Populations

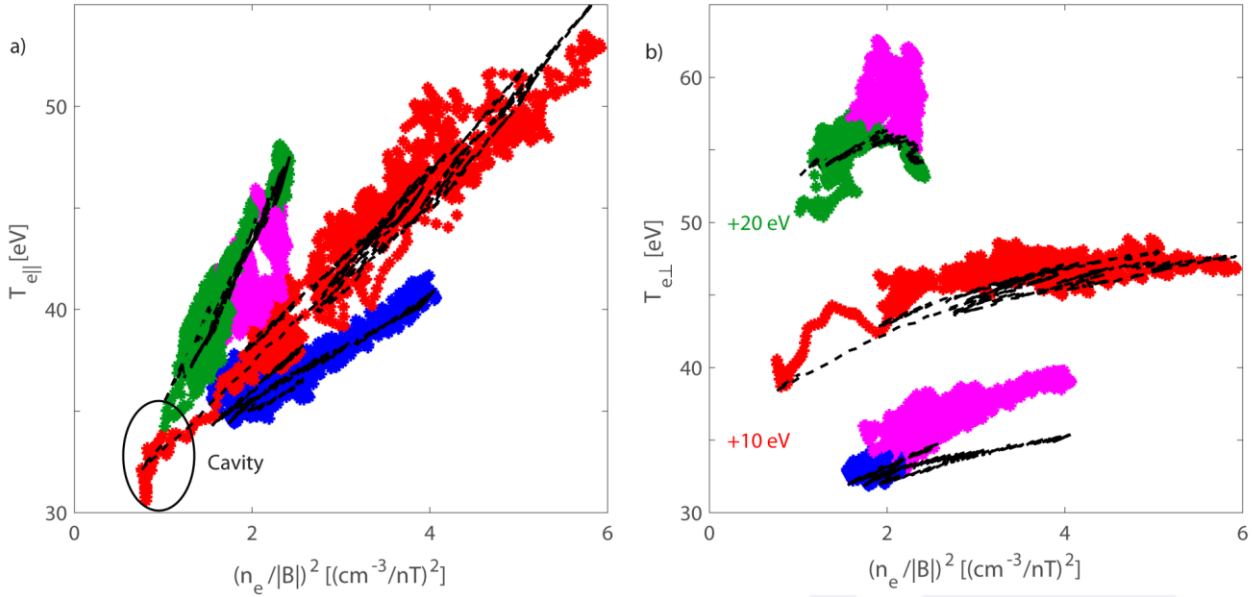

[Wetherton+,JGR:SP, 2021]

Compressing flux tubes

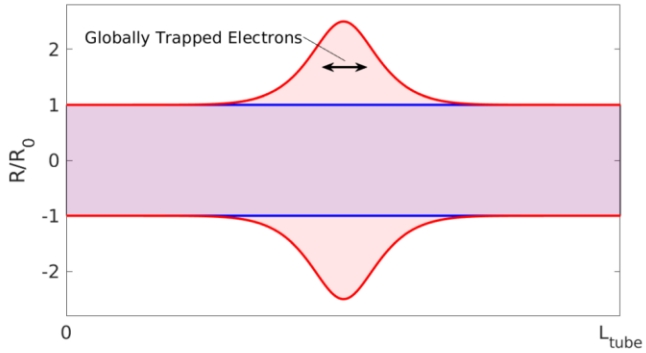

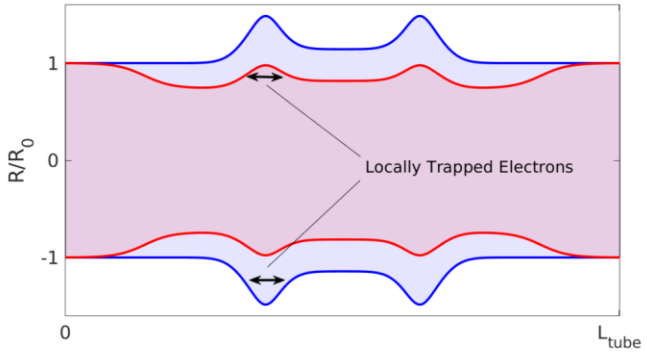

[Wetherton+,JGR:SP, 2021]

Model Extension

- The original model is derived in the limit where the passing electrons have small transit time through the reconnecting region
- Electrons can be energized through nonzero $\int \mu \partial B/\partial t \, \mathrm{d}t$ during compression
- This can be slow transit of passing electrons or trapped electrons that subsequently experience compression
- We add a term in the model to account for this

$$f(\mathbf{x},\mathbf{v}) = \begin{cases} f_\infty(0, \mu B_\infty) & \text{trapped} \\ f_\infty(\mathcal{E} - e\Phi_{\|} - \mu B_\infty - \Delta\mathcal{E}, \mu B_\infty) & \text{passing} \end{cases}$$

Perpendicular heating

[Wetherton+,JGR:SP, 2021]

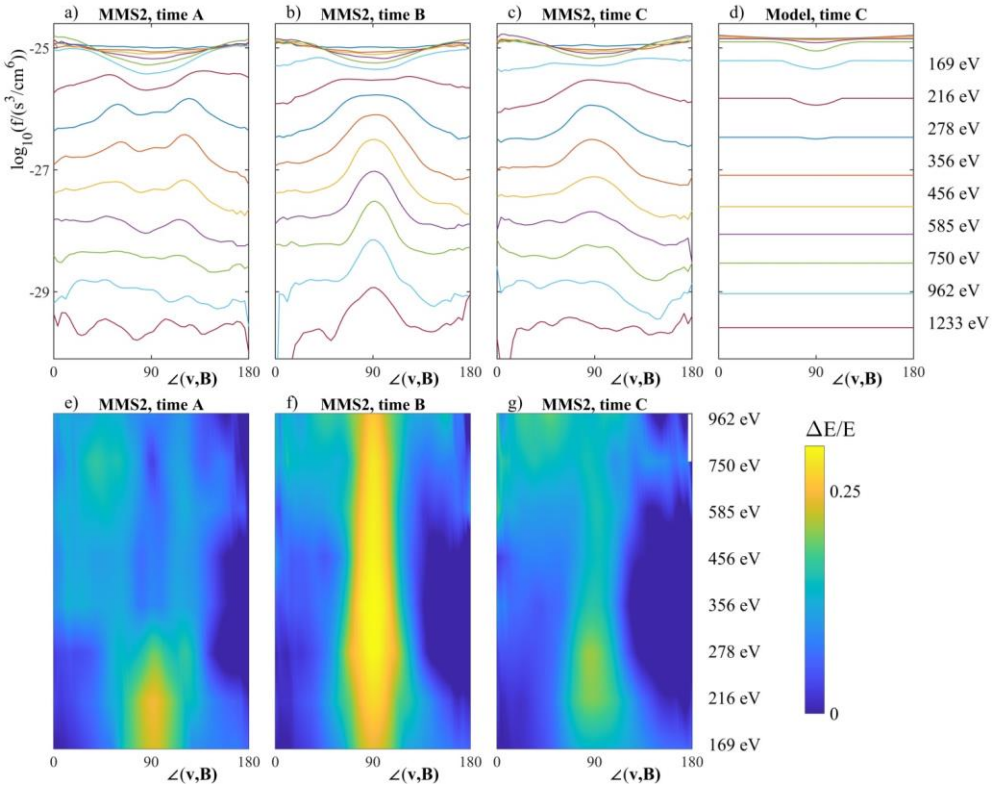

$$f(\mathbf{x},\mathbf{v}) = \begin{cases} f_\infty(0, \mu B_\infty) & \text{trapped} \\ f_\infty(\mathcal{E} - e\Phi_\parallel - \mu B_\infty - \Delta\mathcal{E}, \mu B_\infty) & \text{passing} \end{cases}$$

Perpendicular heating over time

[Wetherton+,JGR:SP, 2021]

$$f(\mathbf{x},\mathbf{v}) = \begin{cases} f_\infty(0, \mu B_\infty) & \text{trapped} \\ f_\infty(\mathcal{E} - e\Phi_\parallel - \mu B_\infty - \Delta\mathcal{E}, \mu B_\infty) & \text{passing} \end{cases}$$

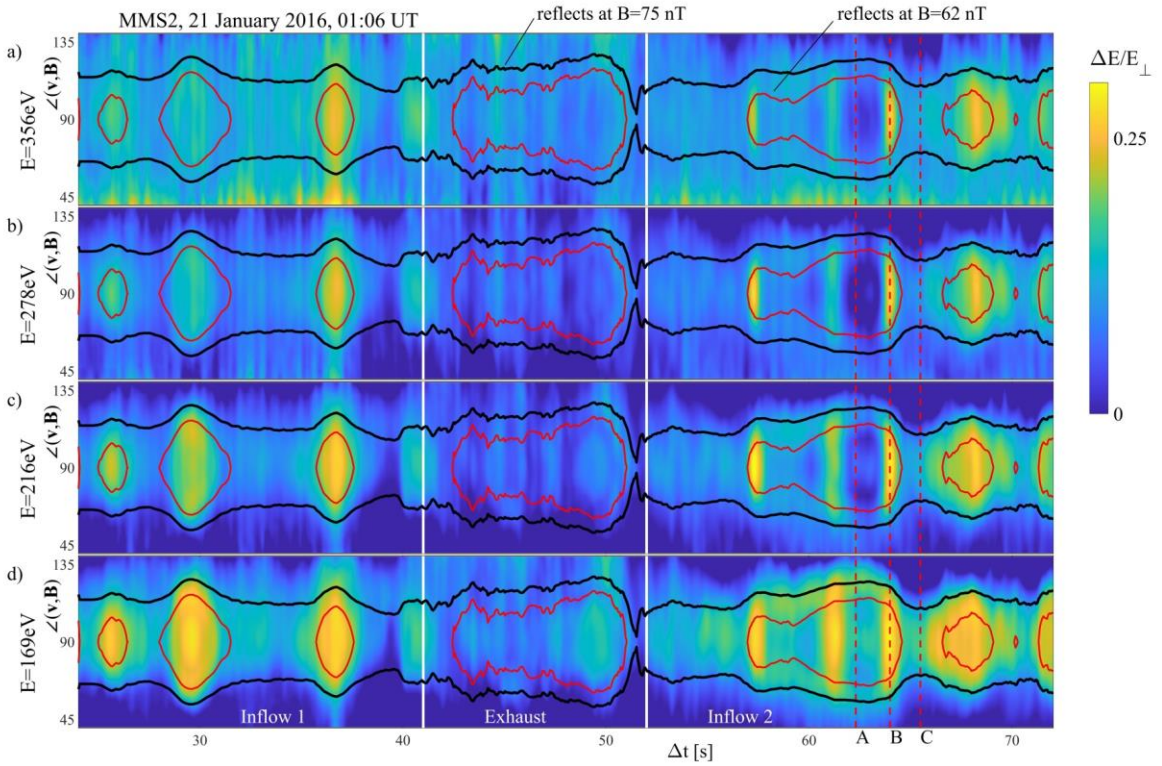

Summary of Event Results

- EoS shown to work far downstream of x-line in MMS event
- Three-pronged parallel temperature characteristics could be an indicator of weakly-asymmetric reconnection
- Model was extended to incorporate the effects of local trapping and ongoing compression

Boltzmann Limit

- For the Boltzmann limit, consider an isotropic upstream distribution in an electrostatic field
- $\frac{df}{dt} = 0 \Rightarrow f(x, \mathcal{E}) = f_\infty(\mathcal{E}_\infty) = f_\infty(\mathcal{E} - e\phi_{||})$
- For a Maxwellian f_∞, $f_\infty(\mathcal{E} - e\phi_{||}) = e^{e\phi_{||}} f_\infty(\mathcal{E})$
- Distribution is scaled by a factor independent of velocity, disregarding trapping effects
- This works for $e\phi_{||} < 0$, but more care must be taken when particles may be trapped

CGL Limit

- For the CGL Limit, all particles are trapped and adiabatic invariants μ and J are conserved
- Estimate $p_{\perp} \sim n \langle m{v_{\perp}}^2 \rangle \sim mn\langle \mu B \rangle \sim nB$
- Estimate $p_{||} \sim n \langle m{v_{||}}^2 \rangle \sim mn \left\langle \left(\frac{J}{L}\right)^2 \right\rangle$
- Mass and flux conservation of a flux tube give $LAn \sim BA \sim constant$, so $L \sim \frac{B}{n}$
- Therefore, $p_{||} \sim mn \left\langle \left(\frac{J}{L}\right)^2 \right\rangle \sim \frac{n^3}{B^2}$
- Alternatively, $T_{||} \sim \frac{n^2}{B^2}$ and $T_{\perp} \sim B$

Hall Fields

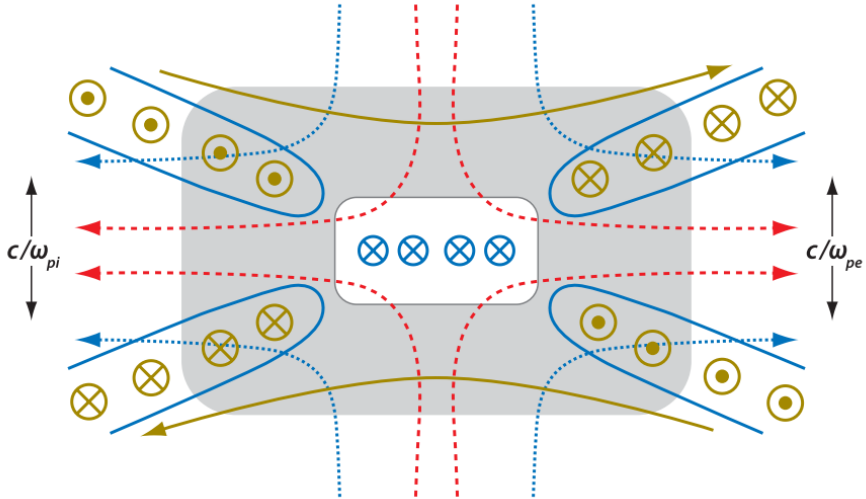

[Zweibel and Yamada 2009]

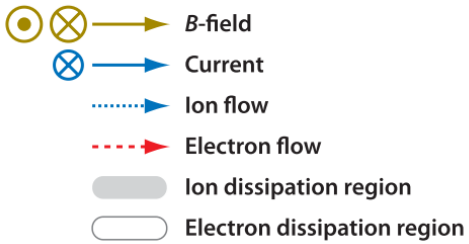

Future Directions

- More complete geometry with central mirror region in fully kinetic and hybrid versions of VPIC
- Add collision models:
  - Model for kinetic ions and fluid electron Coulomb collisions (Lemons et al.) has been implemented
  - DT fusion (e.g., Higginson et al.) has also been implemented
  - Particle Coulomb collision models already exist in VPIC
  - Charge exchange collision models (from J. Jara-Almonte of PPPL) have also been used in VPIC
- Appropriate electron transport equation is a bigger unknown
  - Multi-ion short mean-free path fluid closures are being derived at LANL for magnetized case (see Simakov et al. for unmagnetized case)
- Ad hoc electric field boundary condition may be good enough for initial look at some ion physics

Example Hybrid-VPIC simulations with and without electric potential drop of 5Te

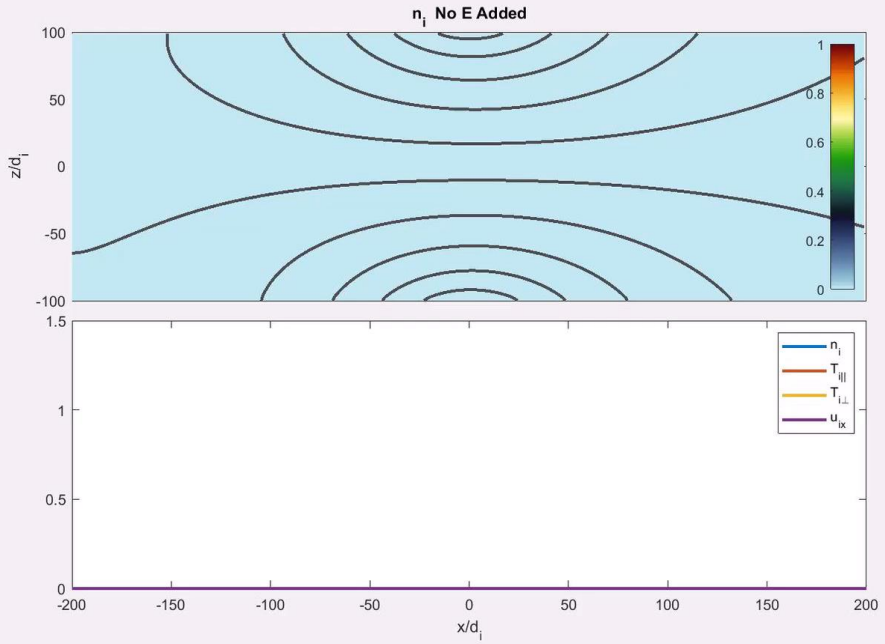

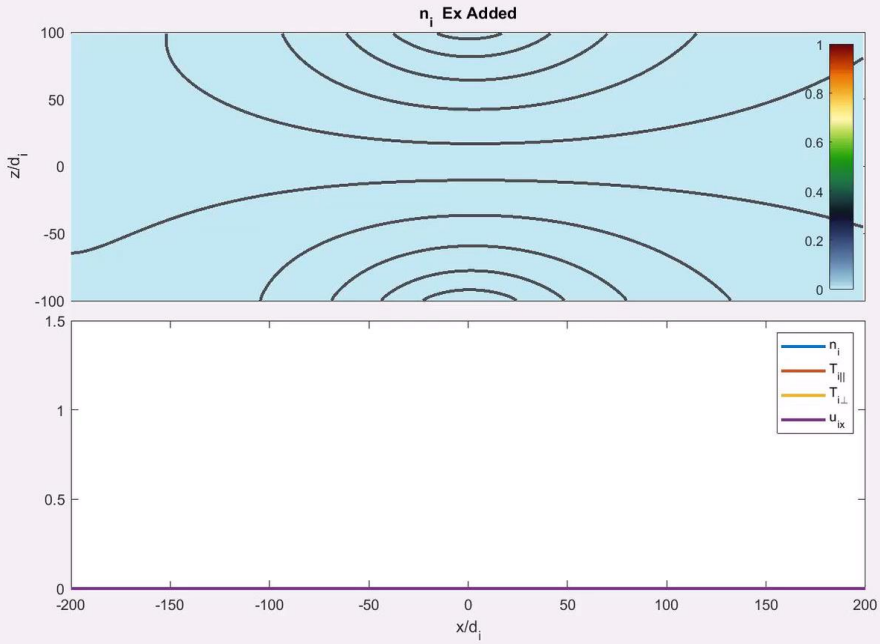

Scaling of the Sheath Potential

- We look at the sheath potential for two values of th filling fraction
- We maintain an internal mirror ratio of 10 and vary over ~ 1 order of magnitude
- We plot both the value of the potential at the last p boundary value
- Sheath potential scales roughly as $(\xi_t R_{ME})^{-3/2}$
- This is a stronger scaling than previously predicted Skovorodin 2019), which could be beneficial for pr

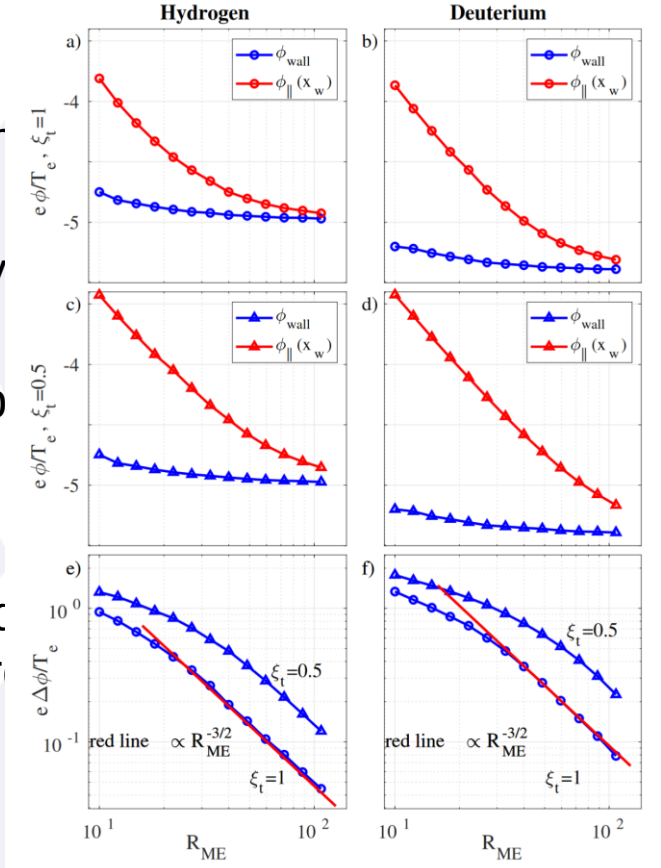

Where is reconnection relevant?

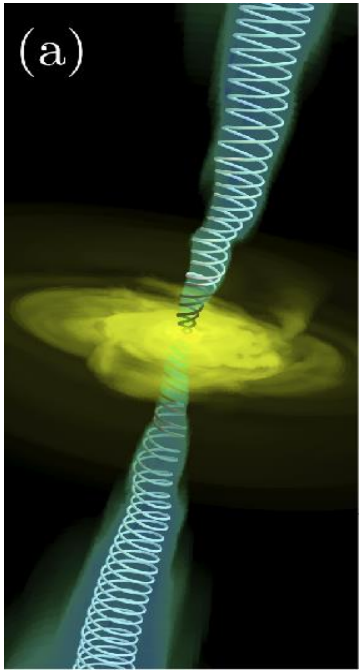

Tchekhovskoy: doi:10.1007/978-3-319-10356-3_3

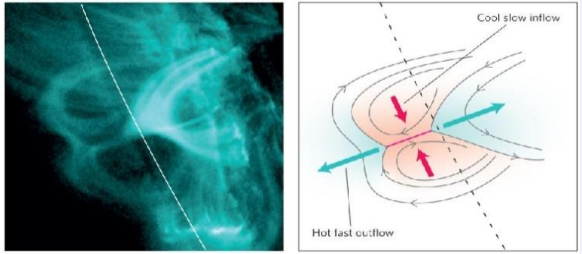

Forbes: doi:10.1038/nphys2703

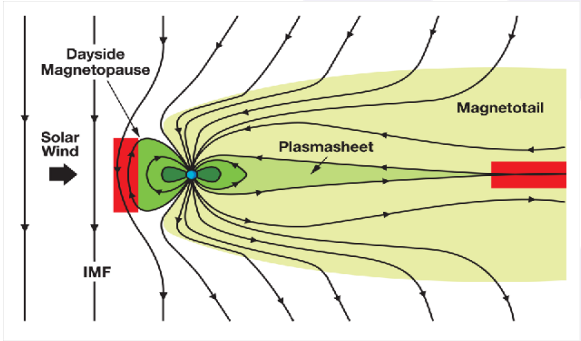

Image: NASA

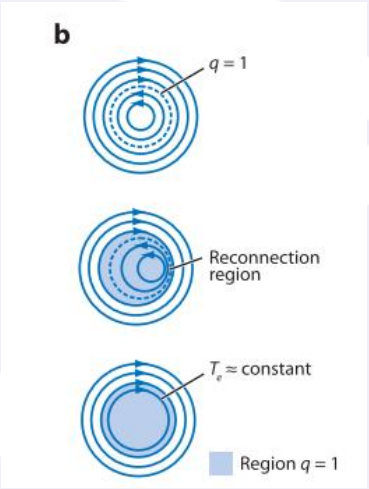

Zweibel and Yamada (2013)

Frozen-in Condition (Alfvén's Theorem)

- The induction equation applied to a flux surface gives

$$\frac{d\psi}{dt} = -\oint \boldsymbol{\nabla} \times (\boldsymbol{E} + \boldsymbol{v} \times \boldsymbol{B}) \cdot d\boldsymbol{S}$$

- For a perfect conductor, flux is frozen to the bulk flow

Breaking the Frozen-in Law

$$\mathbf{E} + \mathbf{v} \times \mathbf{B} = \eta \mathbf{j} + \frac{1}{ne}(\mathbf{j} \times \mathbf{B} - \nabla \cdot \mathbf{p}_e) + \frac{m_e}{ne^2}\frac{d\mathbf{j}}{dt}$$

Sweet-Parker Reconnection

Simplest model for reconnection:

$\mathbf{E} + \mathbf{v}\times\mathbf{B} = \eta\mathbf{j}$ [*Sweet-Parker* (1957)]

Sweet-Parker: L >>δ: $t_{sp} = \sqrt{t_R t_A} = \sqrt{\frac{\mu_0 L^2}{\eta}} \sqrt{\frac{L}{v_A}}$

Unfavorable for fast reconnection

Two months for a coronal mass ejection

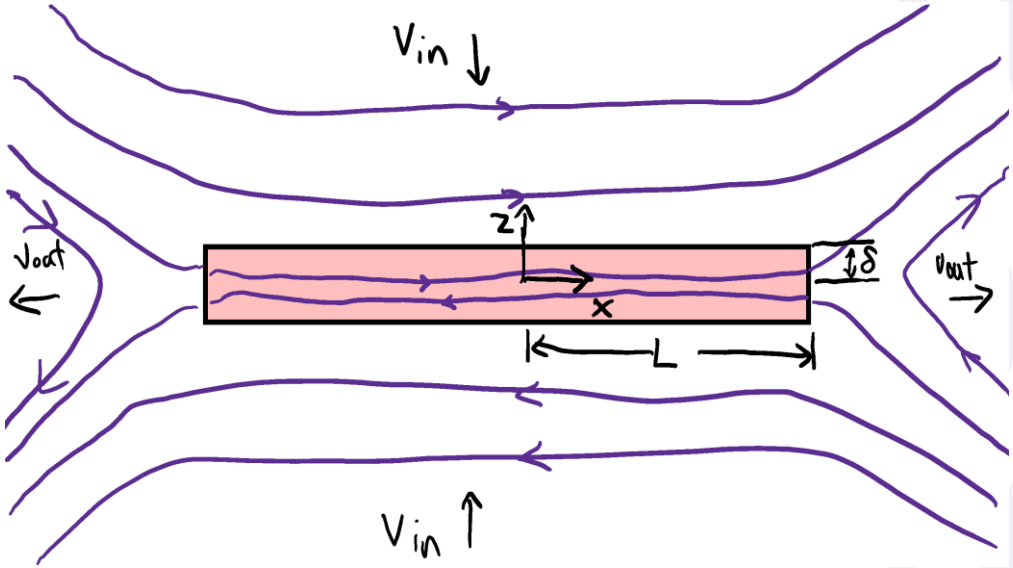

Outflow speed:

$$v_A = \frac{B}{\sqrt{\mu_0 n m_i}}$$

Two-Fluid Simulation

GEM challenge (Hall reconnection)

$\mathbf{E} + \mathbf{v} \times \mathbf{B} = (\mathbf{j} \times \mathbf{B})/ne$ [Birn+, 2001]

Out of plane current

Isotropic pressure

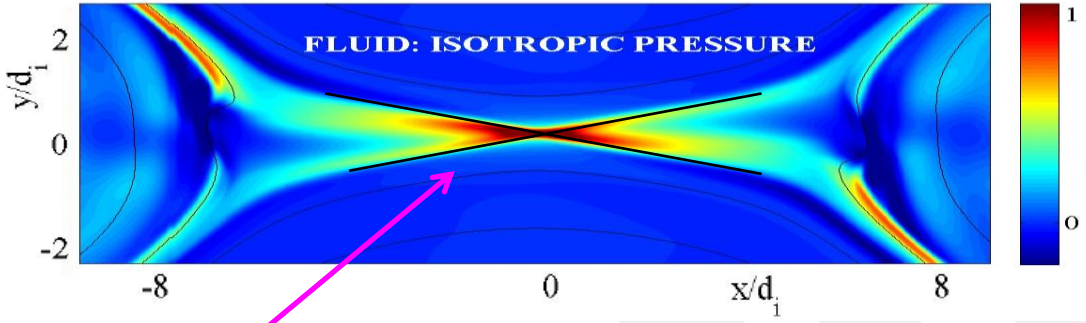

Aspect ratio: 1 / 10

➔ $v_{in} \sim v_A / 10$

Cases of Model Distribution